

The influence of subsurface flow on lake formation and north polar lake distribution on Titan

David G. Horvath^{a,*}, Jeffrey C. Andrews-Hanna^b, Claire E. Newman^c, Karl L. Mitchell^d, Bryan W. Stiles^d

^a Colorado School of Mines, Department of Geophysics and Center for Space Resources, 1500 Illinois Street, Golden, CO 80401, USA

^b Southwest Research Institute, 1050 Walnut St., Boulder, CO 80302, USA

^c Ashima Research, Suite 104, 600 South Lake Avenue, Pasadena, CA 91106, USA

^d Jet Propulsion Laboratory, California Institute of Technology, Pasadena, CA 91109, USA



ARTICLE INFO

Article history:

Received 10 November 2015

Revised 23 April 2016

Accepted 26 April 2016

Available online 3 May 2016

Keywords:

Titan

Titan, hydrology

Titan, surface

ABSTRACT

Observations of lakes, fluvial dissection of the surface, rapid variations in cloud cover, and lake shore-line changes indicate that Saturn's moon Titan is hydrologically active, with a hydrocarbon-based hydrological cycle dominated by liquid methane. Here we use a numerical model to investigate the Titan hydrological cycle – including surface, subsurface, and atmospheric components – in order to investigate the underlying causes of the observed distribution and sizes of lakes in the north polar region. The hydrocarbon-based hydrological cycle is modeled using a numerical subsurface flow model and analytical runoff scheme, driven by a general circulation model with an active methane-cycle. This model is run on synthetically generated topography that matches the fractal character of the observed topography, without explicit representation of the effects of erosion and deposition. At the scale of individual basins, intermediate to high permeability (10^{-8} – 10^{-6} cm 2) aquifers are required to reproduce the observed large stable lakes. However, at the scale of the entire north polar lake district, a high permeability aquifer results in the rapid flushing of methane through the aquifer from high polar latitudes to dry lower polar latitudes, where methane is removed by evaporation, preventing large lakes from forming. In contrast, an intermediate permeability aquifer slows the subsurface flow from high polar latitudes, allowing greater lake areas. The observed distribution of lakes is best matched by either a uniform intermediate permeability aquifer, or a combination of a high permeability cap at high latitudes surrounded by an intermediate permeability aquifer at lower latitudes, as could arise due to karstic processes at the north pole. The stability of Kraken Mare further requires reduction of the evaporation rate over the sea to 1% of the value predicted by the general circulation model, likely as a result of dissolved ethane, nitrogen, or organic solutes, and/or a climatic lake effect. These results reveal that subsurface flow through aquifers plays an important role in Titan's hydrological cycle, and exerts a strong influence over the distribution, size, and volatile budgets of Titan's lakes.

© 2016 Elsevier Inc. All rights reserved.

1. Introduction

The surface of Saturn's largest moon Titan has been extensively modified by processes related to liquid hydrocarbons on the surface. Similar to water on Earth, methane at Titan's surface is near its vapor point and exists in both the gas and liquid phases, suggesting that it is the primary constituent in the hydrocarbon-based hydrological cycle. Ponded liquid on Titan's surface is primarily concentrated around the north polar region

(Stofan et al., 2007) in lakes with variable morphology (Hayes et al., 2008). Lakes with steep-sided and smooth shorelines with no observable fluvial source may be indicative of karst or seepage morphology (Mitchell et al., 2008; Cornet et al., 2015) and can be either liquid filled or empty (Hayes et al., 2008). Larger lakes and seas with irregular shorelines, appear to be located in topographic lows (Stiles et al., 2009) at the terminus of fluvial features (Cartwright et al., 2011; Langhans et al., 2012). Surface modification by fluvial dissection (Burr et al., 2006; Perron et al., 2006; Jaumann et al., 2008; Lorenz et al., 2008a; Burr et al., 2009; Black et al., 2012; Langhans et al., 2012) is driven by precipitation reaching Titan's surface (Tokano et al., 2001).

* Corresponding author. Tel.: +1 5125541461.
E-mail address: dhorvath@mines.edu (D.G. Horvath).

The current orbital obliquity of the Saturn system of 26.7° causes seasonal variations in solar insolation (Lorenz et al., 1999; Stiles et al., 2009), which in turn drives seasonal variations in the polar precipitation and evaporation rates with an annual period of 29.5 years (note that the unit of time “year” will refer to an Earth-year throughout this work, unless specified as a Titan-year). During northern summer, high solar insolation results in atmospheric upwelling at the north polar region, causing rapid cooling of air parcels and condensation of methane to form clouds and precipitation. Observational evidence of cloud formation (Porco et al., 2005) and subsequent darkening of the surface in the south polar region during southern summer (Schaller et al., 2006; Turtle et al., 2011) suggest that convective storm systems bring precipitation to the surface. General circulation models (GCMs) predict increases in the evaporation and precipitation rates (Tokano et al., 2001; Mitchell et al., 2006; Schneider et al., 2012; Lora et al., 2014; Newman, 2015) due to high solar insolation at the polar regions during the summer and spring seasons.

Temporal changes, thought to be due to changes in the distribution of methane on the surface, have been observed at the south polar region and the tropics on Titan. Changes in the surface albedo in the south polar region and tropics are thought to be due to precipitation events and subsequent evaporation (Turtle et al., 2009, 2011). Evidence for temporal changes in the distribution of lakes includes possible present-day changes in the location of the shoreline of Ontario Lacus in the south polar region (Turtle et al., 2011), and dry lakebed morphologies in the north polar region (Hayes et al., 2008) suggesting long-term changes in lake stability. The proposed shoreline change at Ontario Lacus suggests an average loss rate of $\sim 1\text{ m/yr}$ for lakes in the south polar region based on an average shoreline recession of $\sim 2\text{ km}$ (Hayes et al., 2011). However, alternative interpretations have suggested that the spatial resolution of the instrument used was inadequate for determining any measurable shoreline recession (Cornet et al., 2012). While dry lakebed morphologies (Hayes et al., 2008), inferred long-term lake level changes (Stofan et al., 2007; Lucas et al., 2014) indicate long-term changes in lakes, and transient lake features have been observed between subsequent Cassini flybys (Hofgartner et al., 2014), shoreline change in filled northern lakes during the Cassini mission has yet to be observed (Hayes et al., 2011). Based on predicted evaporation and precipitation rates, Mitri et al. (2007) placed theoretical upper limits on lake recession, predicting up to 30 km/yr for shoreline slopes of 0.1% based on altimetric profiles (Elachi et al., 2005). However, that early study required several simplifying assumptions, including constant slope, constant wind speed, and a lack of methane supplied from the surrounding watershed. Hayes et al. (2008) modeled temporal changes in lake area for lakes perched above an aquifer and separated from it by an unsaturated zone, specifically focusing on the timescales for lake disappearance and the influence of aquifer permeability on subsurface and atmospheric exchange of liquid methane. They found that for permeabilities less than 10^{-6} cm^2 , lake recession becomes limited by the evaporation rate and occurs on the order of seasonal timescales. Higher permeabilities, on the order of 10^{-6} cm^2 to 10^{-5} cm^2 , were found to be more consistent with seepage morphology lakes at the north polar region based on the size of these lakes.

Thus, previous work has revealed evidence for atmosphere-surface exchange of volatiles, transport of liquid over the surface, the existence of stable lakes and seas, and possible limited temporal changes in lakes and seas on Titan. Although there is clear evidence for an active hydrological cycle, significant work remains to be done to understand the nature of that hydrological cycle. In particular, the role of subsurface flow in unconfined aquifers, the influence of this flow on the stability and distribution of lakes, and the properties of Titan aquifers are poorly understood. Subsurface hydrology on regional and global scales on Earth and Mars are im-

portant for understanding the distribution and activity of groundwater. A lack of ground truth observations of Titan’s subsurface hydrological properties necessitates comparison of hydrologic models with the observed distribution and behavior of lakes on Titan. While similar in many respects to the water-based hydrological cycles on Earth and Mars, Titan’s hydrocarbon-based hydrological cycle involves a fluid with a lower viscosity and density (depending on the assumed fluid composition), that flows under the influence of a weaker gravitational acceleration on a surface with lower relief, and driven by a longer seasonal cycle. These differences highlight the importance of theoretical studies of Titan’s hydrological cycle.

In this study, we model the full methane-based hydrological cycle of Titan, including atmospheric, surface, and subsurface components. In order to investigate lake behavior on both basin and polar scales, we combined a numerical subsurface hydrology model with an analytical surface runoff model, driven by the outputs from a general circulation model. We compare the results to observations of the distribution and sizes of lakes in order to constrain subsurface properties. In Section 2, the Titan hydrological model is described in detail. In Section 3 we use basin-scale hydrological models driven by precipitation and evaporation rates from a general circulation model at individual latitudes to investigate the behavior of hydrology on Titan at the scale of individual basins. The basin-scale model is then expanded to a polar model extending from the pole to mid-latitudes in Section 4, with latitudinally varying precipitation and evaporation rates. These polar models allow us to investigate the influence of different hydrological parameters on the formation of large seas and the distribution of lakes at the north polar region. The results are compared with observational constraints in the form of the observed lake distribution at the north polar region, and implications for Titan hydrology are discussed.

2. Methods: modeling hydrology on Titan

In order to investigate lake behavior on both basin and polar scales, we developed a numerical model that incorporates the atmospheric, surface, and subsurface components of Titan’s hydrological cycle. The model was run on two-dimensional grids representing the surface topography of either an individual basin or the entire north polar region (Section 2.1). The amount of methane that either recharges the aquifer or channelizes as surface runoff was determined from the outputs of a general circulation model (Section 2.2) using an Earth-based scaling relationship dependent on the precipitation and evaporation potential (defined as the evaporation rate that would occur from a standing body of liquid methane) (Section 2.3). The subsurface flow was modeled using a finite-difference approximation to the groundwater flow equation with parameters appropriate for Titan (Section 2.4). Surface runoff was modeled using a linear reservoir model with parameters appropriate for terrestrial basins (Section 2.5). The model allowed lakes to form and evolve naturally as a result of the balance between the surface, subsurface, and atmospheric fluxes of methane (Section 2.6).

2.1. Topography

Both the gravitationally driven flow of fluids in the subsurface and the surface runoff are dominated by the effects of the surface topography. For this study, we use topography derived from the overlapping antenna beams of the Cassini synthetic aperture radar (SAR) for all Titan flybys up through the T84 flyby (Stiles et al., 2009). The total relief (referenced to the geoid) on Titan is $\sim 2.5\text{ km}$, while the relief on smaller scales relevant to the basin-scale hydrological modeling in this study is $\sim 1.4\text{ km}$ (Fig. 1). In an

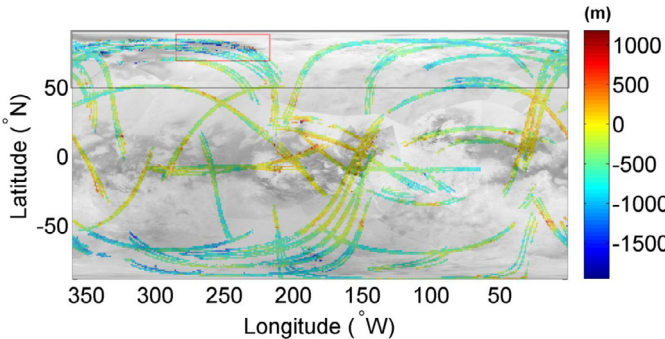


Fig. 1. Global coverage of the synthetic aperture radar topography (Stiles et al., 2009) overlain on global Cassini Imaging Science Subsystem (ISS) mosaic (image credit: NASA/JPL-Caltech/SSI, http://astrogeology.usgs.gov/search/map/Titan/Cassini/Global-Mosaic/Titan_ISS_P19658_Mosaic_Global_4km). The red box surrounds Ligeia Mare, the region of interest for the basin-scale models, and the black box encompasses the north polar lake region of interest for the polar models.

unconfined aquifer, where the methane table generally follows a diffused representation of the surface topography, low relief will cause lower hydraulic gradients, thereby decreasing the rate of subsurface flow. Furthermore, as a result of the low relief on Titan, fluid at greater depths will not significantly affect the surface hydrological cycle.

The limited surface topography available for Titan (Stiles et al., 2009; Fig. 1) is inadequate for direct hydrological modeling of specific regions, with the exception of a few areas for which stereo-SAR coverage exists (Kirk et al., 2013). We circumvent this limitation using synthetic topography. Surface topography is often approximately self-affine, behaving in a fractal nature (Mandelbrot et al., 1982). This self-affine nature allows for a statistical measure of surface topography to be calculated from individual topography swaths across specific regions of interest. The fractal nature of the surface topography can be quantified by the Hurst exponent (Campbell, 2002), which describes how the variance in elevation of points separated by a given distance depends on that distance. The Hurst exponent is calculated as half the slope of the log of the distance-dependent variance in elevation as a function of the log of the distance. The Hurst exponent calculated from two-dimensional SAR topography (Stiles et al., 2009) or radar altimeter swaths (Elachi et al., 2005) can be used to generate synthetic fractal terrain that is statistically similar to the observed landscape, but is sampled over a dense two-dimensional grid suitable for hydrological modeling. The variance in elevation as a function of the distance between two points in a single SAR topography profile was determined and binned at different distance scales. The slope (Hurst exponent) and intercept of the best-fit line to the log of the variance in elevation as a function of the log of the distance were then used as inputs to the fractal generation algorithm. In this representation, a slope of 1 indicates perfectly self-affine behavior. While processes such as erosion, deposition, and dissolution of material can produce surfaces that are not self-affine, some large north polar lake shorelines appear fractal (Sharma and Byrne, 2010), indicating that the surrounding topography can be approximated by a fractal surface. Small steep-sided depressions that make up the majority of lakes at the north polar region appear to have rounded shorelines that formed due to dissolution. In this work, we focus on the large north polar seas and assume a fractal terrain surrounding these large basins. Our analysis below of individual topography swaths further supports the fractal nature of the topography at scales relevant to this work. Future work will consider departures from a fractal landscape as a result of the modification of the surface by erosion, deposition, and dissolution.

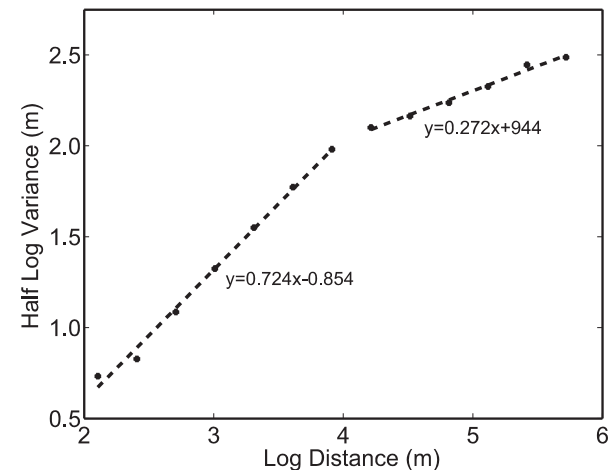


Fig. 2. The log of the distance dependent deviation as a function of the log of the distance from SAR topography over the region surrounding Ligeia Mare (solid circles) and the best fit line to the data (dashed lines). A two-slope fit provides the best fit to the data with a break at 10 km.

We focus our basin-scale topographic analysis on an area in the north polar region in the vicinity of Ligeia Mare. The fractal analysis in this region yielded a two-slope fit for the Hurst exponent. At distance scales less than 10 km, a slope and intercept of 0.724 and -0.854 were calculated, while at scales greater than 10 km a slope and intercept of 0.272 and 0.944 were calculated (Fig. 2). The greater slope of the fit at scales less than 10 km indicates that the topography displays a more self-similar nature than at scales greater than 10 km. We note that the effective footprint of the SAR topography of ~ 9 km (Stiles et al., 2009) may bias the Hurst exponent at scales smaller than this, but our model results are insensitive to the relief at these finer scales. The north polar region is relatively rougher than other regions on Titan (Stiles et al., 2009) possibly due to the enhanced hydrological activity and erosion at high northern latitudes. For the polar models, topographic statistics were determined at 15° latitude increments from 45°N to the pole. As in the case of the topography in the region surrounding Ligeia Mare, a two-slope fit with the break at 10 km provided the best fit to the data. Slope values for scales greater than 10 km suggest a decrease in self-similarity moving north towards the pole with slope values of 0.384, 0.114, and 0.113 for latitudes between 45° and 60°N, 60° and 75°N, and 75° and 90°N, respectively. At distance scales less than 10 km, slope values remained consistently around 0.7, again suggesting a more self-similar terrain at shorter scales.

Synthetic topography was generated using a diamond-square fractal generation algorithm (Fournier et al., 1982). This method takes an initial square, defined at the four corners of the topographic domain, and generates a topographic value in the center of the square using a random perturbation from the mean of the four corners that depends on the distance from the computational node to the corners, and the slope and intercept derived from the distance-dependent variance based on the SAR topography profiles. The diamond step utilizes the newly generated center elevation and the four corner pairs (NW-NE, NE-SE, SE-SW, SW-NW) to generate topography at the central north, east, south, and west nodes, respectively. This process is repeated until a two dimensional synthetic topographic map has been generated (Fig. 3).

For the basin-scale models, a purely synthetic fractal topography grid with a central depression was used to model a closed topographic depression. Because our primary interest is in the nature of the lake, a central depression was imposed on the grid rather than allowing it to form at a random location. An initial 3×3 grid

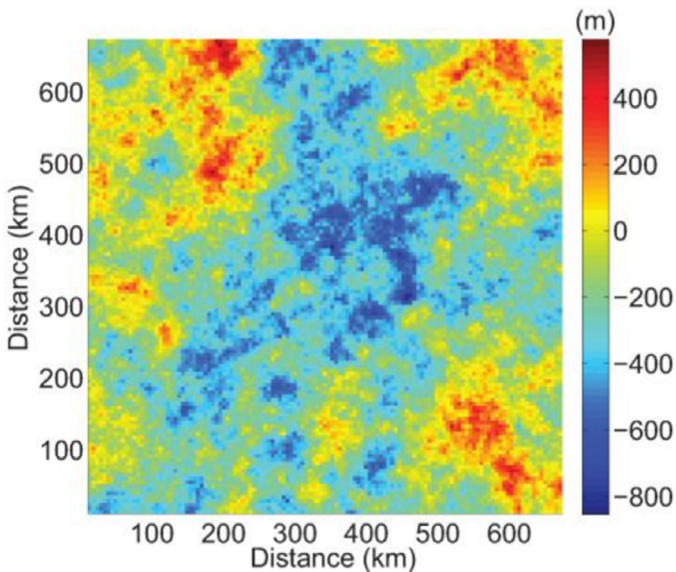


Fig. 3. Fractal topographic map for the basin-scale modeling, generated based on the fractal properties of the SAR topography data over the region surrounding Ligeia Mare.

of points was determined by generating a coarse grid landscape at a distance spacing equivalent to half the length of the model domain and then selecting a central low point such that the distance dependent variance was preserved. For the polar models, in order to provide a direct representation of the north polar region, an interpolation algorithm using the SAR topography was included in the fractal generation (Fig. 4a). This algorithm used an inverse distance-squared weighting interpolation to generate a 2×2 grid of points from the existing topography data that acted as the initial inputs to the fractal algorithm. In the subsequent fractal generation algorithm, if the distance from a computational node to an observed elevation point was less than the distance to the four square or diamond points, the data point was used in the fractal algorithm along with the corner points with an inverse distance-squared weighted. This method fits the SAR topography data while preserving the fractal nature of the landscape (Fig. 4b).

The fractal algorithm alone, though, does not account for the location of the large basins containing seas at the north polar region. Thus, these basins were imposed in the polar topography models. Using the Cassini radar map of the north polar region, the four largest seas (Kraken Mare, Ligeia Mare, Punga Mare, and Jingpo Lacus) were masked out and an elevation threshold was applied to each individual sea based on the average SAR topography elevation value at each lakes shoreline. In the fractal algorithm described above, a point within one of the seas was rejected if the elevation was above the average shoreline value, or accepted if the elevation was below the average shoreline value. This method forms broad topographic lows where the four largest seas are located, while still maintaining the fractal nature of the surrounding topography within and surrounding the imposed basins.

We note that the evolution of a landscape subjected to a hydrological cycle through the processes of erosion and deposition of material has an impact on the resultant hydrology. Well-developed fluvial systems will transport fluids rapidly from source to sink. Erosion and deposition can result in systematic variations in the slope and fractal character of the relief within a catchment. This study is limited by the sparsely sampled topography data available to us. Although our synthetic topography matches the fractal character and overall relief of the Titan landscape, while also reproducing known basins surrounding large seas, it cannot repro-

duce the exact nature of Titan's relief. However, results of landscape evolution models indicate that fluvial erosion has resulted in only slight (< 9%) changes to the surface topography (Black et al., 2012), and the density of drainage networks is generally low (Burr et al., 2013), supporting our use of a simple fractal surface. To test the effect of a more evolved Titan landscape, models were run (not shown) in which runoff was controlled by a diffused representation of the surface topography, which acts to smooth over local lows and increase the size of catchment areas. These models yielded similar results to the models in which runoff was controlled by the original fractal topography.

2.2. General circulation model

The general circulation model (GCM) used for this study (Newman et al., 2011; Newman, 2015) is a global adaptation of the terrestrial Weather, Research, and Forecasting (WRF) model described in detail by Richardson et al., (2007). In contrast to the limited area of the original WRF model, TitanWRF (and the more general PlanetWRF) uses a global atmospheric model that accounts for planetary scale physics. For Titan specifically, visible and near infrared absorption by methane, Rayleigh scattering, and haze particle scattering are accounted for. The GCM utilized for this study (Newman, 2015) limited liquid methane at the surface by allowing individual cells to dry out if evaporation exceeded precipitation over time, and included the latent heat effects for methane vaporization, but lacked topographic effects. The GCM output was at a spatial resolution of 5.625° longitude by 5° latitude and a temporal resolution of 128 days. While shorter time steps were investigated, because of the longer timescales for subsurface flow, higher frequency GCM outputs had little effect on the seasonal stability and distribution of Titan lakes. The GCM was initialized with uniform surface methane and then run until its methane cycle reached equilibrium – i.e., until the annual-mean surface methane distribution remained roughly constant from year to year. By this point in the GCM the low and mid latitude surface was dry except for transient surface methane immediately following precipitation events, with long-term surface methane remaining only poleward of $\sim 75^\circ$ N. After equilibration of the GCM, the Titan-yearly time series of longitudinally averaged potential evaporation (E_p) and precipitation (P) were then determined from the average of an 18 Titan-year GCM simulation and used as the inputs to the hydrology models. The potential evaporation was determined using a mass transfer equation given in general form as:

$$E_p = C_u \Delta q \quad (1)$$

where C_u is a density-weighted exchange coefficient related to the surface wind stress and Δq is the difference between the actual and saturated specific methane humidity. Fig. 5 shows E_p and P for a range of latitudes, averaging over all longitudes. Note that the large increase in E_p at 75° N coincides with the boundary between a generally methane-free and methane-covered surface in the GCM. This sharp transition is due in part to the effect of evaporative cooling, which decreases the surface temperature in the polar region and reduces further evaporation.

The GCM outputs used for this work encompass hyper-arid climates below 75° N down to 45° N, with an average precipitation rate of 2.37 cm/yr and an average evaporation potential of 635 cm/yr , to semi-arid climates above 75° N, with an average precipitation rate of 5.79 cm/yr and an average evaporation potential of 11.23 cm/yr . During northern summer and spring, an increase in the solar insolation causes higher evaporation potential and highly variable precipitation rates around the pole, while northern winter predicts lower evaporation potential and precipitation rates. At latitudes $> 75^\circ$ N, summer and spring precipitation rates range from $< 1 \text{ cm/yr}$ to 54.7 cm/yr with an average precipitation rate of

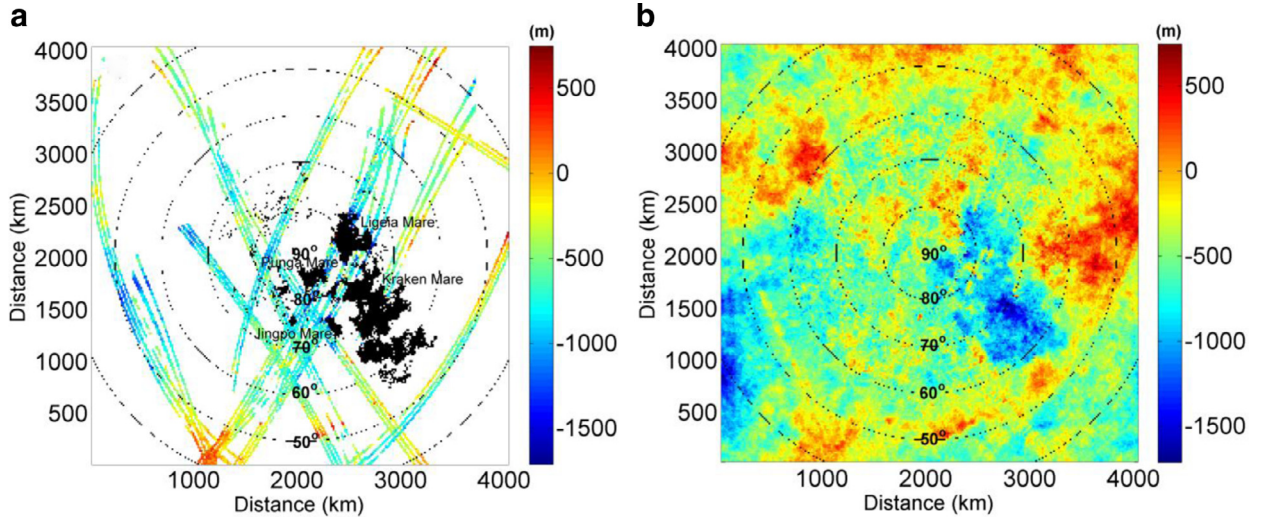


Fig. 4. The SAR topography at the north polar region used in the interpolation algorithm overlain by lakes (black) mapped from the Cassini radar map of the north pole (a) and the fractal topographic map with an interpolation algorithm and imposing Kraken Mare, Jingpo Mare, Ligeia Mare, and Punga Mare centered at 0°W longitude (b).

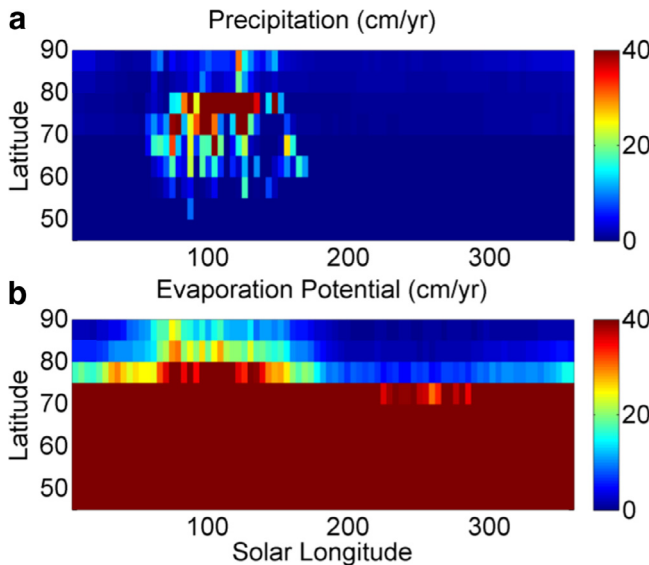


Fig. 5. Precipitation rates (a) and evaporation potential (b) from the general circulation model from 45°N to 90°N over a Titan year. Evaporation potential is saturated in the panel (b) at lower latitudes to highlight the variability at high latitudes but reaches values greater than 1000 cm/yr.

10.1 cm/yr and an average evaporation potential of 18.5 cm/yr. The winter months are characterized by low precipitation and evaporation potential, and an E_p/P ratio closer to 1. Hyper-arid climates below 75°N are characterized by high evaporation potentials and little change in precipitation over the course of a Titan year.

The hydrological modeling in this work (see Section 2.4 below) allows methane to flow in the subsurface between latitudes and in some cases to evaporate from or even pond on the surface at lower latitudes where no stable surface methane is predicted by the GCM. However, the evaporation potential and precipitation outputs from the GCM were not coupled to the hydrology model and thus lacked the inherent feedbacks between the deep subsurface and atmospheric components of the hydrological cycle. For example, the subsurface flow of methane to drier low latitudes, below 60°N, would result in evaporative cooling and decreased evaporation rates relative to the evaporation potential predicted by the GCM. These decreased evaporation rates could allow stable lakes

to form at lower latitudes. These limitations could only be resolved with a fully coupled land and atmosphere model, which is beyond the scope of this work. Nevertheless, in simulations with realistic rates of recharge and runoff at the high polar latitudes, the low rates of subsurface flow to the lower latitudes result in evaporation rates that are much lower than the predicted evaporation potential rates and thus would be unaffected by a modest decrease in the evaporation rate due to evaporative cooling.

2.3. Aquifer recharge and runoff generation

Precipitation that reaches the surface can infiltrate and percolate downward to the methane table, exceed the infiltration capacity and generate runoff, evaporate from the bare soil surface, or remain in the soil and/or unsaturated zone. These behaviors are controlled by processes at scales much smaller than the resolution of the subsurface hydrology model used in this study, and rely on poorly constrained parameters for Titan such as soil properties and soil thickness. In order to capture the nature of these processes occurring at the interface between the atmospheric and surface components of the hydrological cycle, we adopted a simple empirical method used in terrestrial hydrology. Budyko-type methods (Budyko, 1974) approximate these micro-scale processes on a basin-scale using empirical discharge data from terrestrial basins to derive a functional relationship dependent on the aridity index (ϕ), defined as the ratio of the mean annual evaporation potential and the mean annual precipitation. Earth-based studies (McMahon et al., 2011) have shown that for basin-scale hydrology over long periods, this functional relationship takes the form:

$$F(\phi) = 1 - e^{(-\phi)} \quad (2)$$

where F is the fraction of precipitation that evaporates directly from the surface and does not contribute to recharge or overland flow. Using this functional relationship, the precipitation and aridity index can be used to calculate the recharge and runoff generation as a function of time, t :

$$I(t) = P(t)[1 - F(\phi)] \quad (3)$$

where $I(t)$ is the excess precipitation that will become either surface runoff or aquifer recharge. The simple form of Eq. (2) is useful because it allows easy scaling to account for the possibility of different behavior of methane on Titan in comparison to water on Earth, as is discussed below.

Although the Budyko-type relationship in Eq. (2) generally holds for Earth, it may not apply directly to Titan. The liquid methane interaction with both the ice grains and mantling solid organics will have a controlling effect on the fraction of the precipitation that will participate in the surface and subsurface hydrology rather than evaporate directly back into the atmosphere. To account for this uncertainty, models were also run in which the Budyko-type relationship was modified to either increase or decrease the fractional amount of precipitation excess. This variability was modeled by adding an arbitrary scaling factor to the aridity index in the exponent (Eq. (1)), with the limiting case of a scale factor of zero, allowing all precipitation to contribute to the surface and subsurface hydrology.

The excess methane precipitation (as determined by the scaled Budyko-relationship) is partitioned into methane that recharges the methane table, and methane that contributes to the surface runoff by means of shallow subsurface flow, flow through a partially saturated soil layer, and direct overland flow. On Earth, the partitioning of excess precipitation between aquifer recharge and surface runoff is dependent on the soil and subsoil layer thicknesses, the slope of the land, the total upslope area discharging to a specific region, the rate of precipitation during a rainfall event and the permeability of the soil. Depending on the properties of the soil and subsoil layers, the recharge to the aquifer can range from a negligible fraction of the excess precipitation in the case of a saturated clay layer or exposed bedrock, to nearly all of the excess precipitation in the case of a highly permeable sand layer. The permeability of soil on Earth is largely controlled by the grain size of the soil and the amount of organic material it contains. The regolith on Titan likely contain a mixture of ice grains and solid organics (Lorenz et al., 2008b), though it is unknown if these organics would play a similar role to those in soils on Earth. The Huygens probe landed in the equatorial region of Titan and found a mixture of solid organics at the surface (Niemann et al., 2005). Results from mechanical probing of the surface substrate were consistent with a tar-like material, possibly similar to a saturated soil or a lightly packed snow on Earth (Zarnecki et al., 2005). The nature of the interaction of liquid hydrocarbons with the ice and solid hydrocarbons that mantle the surface is unknown, and will have a controlling effect on the amount of recharge to the aquifer. Due to the poor constraints on the subsurface properties, the unknown nature of the interaction of the liquid with the regolith on Titan, and the large spatial and temporal scales used in this model, recharge and runoff fractions were homogenously set over the entire domain and varied between 0 and 1 to investigate the sensitivity of the results to these parameters. Spatially and temporally varying recharge and runoff fractions were also investigated but found to have little effect on the results given the long temporal and spatial scales of interest in this study.

2.4. Fluid flow through a porous medium

Once methane has infiltrated into the subsurface and reached the methane table, it will contribute to subsurface flow in an unconfined aquifer. Subsurface flow through a porous medium was modeled using a finite-difference approximation of the groundwater flow equation in an unconfined aquifer. The lateral flow of fluid in an aquifer depends on the active aquifer thickness (b), the hydraulic conductivity (K), the porosity (n) and the hydraulic gradient ($\partial h/\partial x$):

$$\frac{\partial}{\partial x} \left(K_x b \frac{\partial h}{\partial x} \right) + \frac{\partial}{\partial y} \left(K_y b \frac{\partial h}{\partial y} \right) = n \frac{dh}{dt} \quad (4)$$

where the active aquifer thickness b varies in space and time as a function of the hydraulic head h and the topography z :

$$b(x, y) = h(x, y, t) - z(x, y) + d \quad (5)$$

in which d is the total thickness of the aquifer (assumed to be a constant value of 10 km).

The hydraulic conductivity describes the ability of a fluid to flow through a medium, and is a function of the aquifer permeability (k), the kinetic fluid viscosity (μ), the fluid density (ρ), and the gravitational acceleration (g):

$$K = \frac{k \rho g}{\mu} \quad (6)$$

While liquid on Titan is a likely mixture of multiple constituents (Brown et al., 2008), methane and ethane are thought to be the most abundant and to control the physical properties that govern fluid flow. At the northern polar region, methane is likely the dominant fluid participating in the fluvial dissection and atmospheric component of the hydrologic cycle (Tan et al., 2013; Mitchell et al., 2015) and a pure methane fluid in the subsurface was assumed for this work. At Titan surface conditions, methane is less dense (450 kg/m³) and less viscous (2×10^{-4} Pa-s) than water on Earth (Lorenz et al., 2003). The low gravitational acceleration on Titan (1.35 m/s²) decreases the rate at which fluid will flow compared to flow under otherwise similar conditions on Earth. The opposing effects of the decreased density and gravity, and the decreased viscosity partially cancel out. For a given permeability, the hydraulic conductivity of an aquifer on Titan will be a factor of ~ 3 lower than that of an identical aquifer on Earth.

$$\frac{K_{\text{Titan}}}{K_{\text{Earth}}} = \frac{\rho_{\text{methane}} g_{\text{Titan}} \mu_{\text{water}}}{\rho_{\text{water}} g_{\text{Earth}} \mu_{\text{methane}}} \approx \frac{1}{3} \quad (7)$$

The permeability of a porous medium is controlled by the size, shape, and interconnectivity of the pore space and fractures in the medium. Titan's surface is composed of water ice "bedrock" overlain by "soil" that is likely composed of a mixture of ice grains and organics of atmospheric origin (Lorenz et al., 2008b), compared to silicate-based bedrock and soil composed of a mixture of silicate grains and organics of biological origin on Earth. Although the composition of Titan's surface is different from Earth, the physical properties governing the flow through the porous media may be similar in aquifer systems. Flow through the soil layer is controlled by the grain size, and the presence of widespread sand dunes on both Earth and Titan supports similar, or at least overlapping, grain size distributions of some of the materials at the surface. Flow through the crystalline crusts of both Titan and Earth would occur dominantly through fractures, whose apertures as a function of depth are determined by the fractal nature of the fracture surfaces. Fracture apertures on Earth follow a predictable decrease with depth irrespective of host rock lithology (Snow, 1970), allowing for generalized permeability models for Mars (Hanna and Phillips, 2005) and Titan. The reduced Young's modulus of ice (Gammon et al., 1983) would likely lead to more rapid closure of fractures with depth, which may cancel out the effect of the lower gravity on Titan.

Permeability values can span orders of magnitude in terrestrial aquifers, and there is no reason to believe that aquifers on Titan would be fundamentally different or fall outside the range of values encountered on Earth. Here we use a range of permeability values representative of terrestrial aquifers. We assume a laterally homogenous aquifer in which the vertically averaged permeability has an exponential dependence on the depth of the methane table:

$$k(h) = k_0 e^{-(z-h)/z_0} \quad (8)$$

where k_0 is the vertically averaged permeability when the methane table is at the surface and z_0 is a scale height which we assume to be 5 km. After scaling for effective stress ($(\rho_{\text{rock}} - \rho_{\text{fluid}})g$), this scale height is equivalent to 0.2 km on Earth, which is less than the value for Earth of ~ 1 km from an exponential fit to the model

of Manning and Ingebritsen (1999) between 1 and 5 km depth, but greater than the equivalent scale height after correcting for the smaller Young's Modulus of ice relative to rock (~ 0.1 km). Permeability values on Earth commonly range between 10^{-16} and 10^{-4} cm 2 (Heath, 1983), with typical values for unconsolidated sand of 10^{-9} to 10^{-4} cm 2 , for sandstones of 10^{-12} to 10^{-8} cm 2 , for carbonate rocks of 10^{-10} to 10^{-4} cm 2 , and for igneous aquifers of 10^{-16} to 10^{-7} cm 2 . In this study, we examine values of the vertically averaged permeability when the methane table is at the surface of 1×10^{-6} cm 2 (corresponding to a permeability at the surface of $k_{surf} = 2.3 \times 10^{-6}$ cm 2), 1×10^{-8} cm 2 ($k_{surf} = 2.3 \times 10^{-8}$ cm 2), and 1×10^{-10} cm 2 ($k_{surf} = 2.3 \times 10^{-10}$ cm 2). For the purpose of discussion, we will refer to these as high (comparable to a fractured bedrock aquifer), intermediate (comparable to an unfractured sandstone or a slightly fractured granite aquifer), and low permeability (comparable to a consolidated bedrock aquifer), respectively. Models run using permeability values an order of magnitude higher and lower than the highest and lowest permeability values were found to have little effect on the overall results, and thus justify the choice of permeability range used in this work. As will be shown below, the results favor the intermediate permeability models, obviating the need to consider higher and lower values outside of this range. We note that this range of assumed permeability values over four orders of magnitude exceeds the likely range of viscosities of hydrocarbon mixtures in the subsurface of Titan (Lorenz et al., 2010; Hayes et al., 2013), and thus the specific fluid composition and viscosity has only a secondary effect on our conclusions.

While a laterally homogenous aquifer is assumed for this study, most aquifers on Earth are not homogenous. Studies have found that smaller scale heterogeneities within the aquifer have little influence on the regional scale flow (e.g., Freeze and Witherspoon, 1967), suggesting that heterogeneities will have little effect at the spatial scales used in this work. The use of a single average aquifer permeability throughout the entire domain allows the investigation the influence of different aquifer properties on the hydrology and formation of lakes. The potential for karst morphology on Titan (Mitchell et al., 2008; Cornet et al. 2015) suggests that focused high permeability pathways and interconnected cave systems may exist on Titan. A karst aquifer system can influence the distribution of methane and the subsurface hydrology, and may not be properly modeled as Darcy flow. However, flow in cave systems behaves more like overland flow, which is included in our model, rapidly redistributing subsurface methane. Models in which all of the precipitation contributes to runoff rather than recharge may approximate a well-developed karst system. Further discussion of the influence of focused flow paths and hydrologic settings are found in Section 4.3.

The porosity is assumed to follow a similar exponential relationship to that assumed for the permeability

$$n(h) = n_0 e^{-(z-h)/d} \quad (9)$$

in which the same scale height of 5 km is used. On Earth, the effective elimination of pore space and permeability with depth is dominantly a result of pressure solution rather than elastic compaction (Renard et al., 2000). On Titan, it is unknown what processes controls the variations of permeability and porosity with depth. However, since the total range of relief in our models is typically < 2 km, the decrease in porosity and permeability with depth has only a minor impact on the subsurface flow and different scale heights would not significantly alter our results. We assume a maximum aquifer depth of $d_{max} = 10$ km (equivalent to a depth of ~ 0.4 km on Earth by simple effective stress scaling). However, our results will not be sensitive to this choice for any maximum aquifer depth that is substantially greater than the typical vertical relief on Titan of ~ 2 km. Furthermore, the deepest portions

of the aquifer will have little effect on the total flow due to the low porosity and permeability resulting from the assumed exponential relationships.

2.5. Surface runoff

Some fraction of the methane falling on the surface from precipitation will contribute to runoff and aquifer recharge, as determined using the Budyko-type method described above. While multiple processes may control runoff and channelized flow on Titan's surface (Burr et al., 2013), the large time steps associated with numerical subsurface modeling in comparison with the timescales for dynamic surface runoff necessitate the use of a simple analytic approximations to represent runoff. In drainage basins on Earth, the precipitation excess does not instantaneously discharge at the outlet, but will be delayed by a storage component dependent on the size and slope of the catchment. For this study, a linear reservoir approximation is used to determine surface runoff based on the assumption that the amount of liquid stored in a catchment is linearly related to the amount of surface runoff (Cunge, 1969; Overton, 1970; Dooge, 1973)

$$S = KQ \quad (10)$$

where S is the storage in the catchment in kilometers (equivalent to the average depth of methane across the catchment), Q is the surface runoff in kilometers per hour, and K is the storage coefficient in hours. Studies have found that the storage coefficient (K) is related to the time between the initial precipitation event and the peak runoff at the catchment outlet (Overton, 1970):

$$K = \frac{t_c}{2} \quad (11)$$

where t_c is the concentration time for a catchment defined as the time it takes a parcel of liquid to travel the length of a catchment. The change in catchment storage over time is determined by the balance between the excess precipitation in the basin and the surface runoff at the basin outlet

$$I(t) - Q(t) = \frac{dS}{dt} \quad (12)$$

where I is the fraction of the excess precipitation that will runoff determined using the Budyko-type method. Combining Eqs. (10)–(12) yields:

$$I(t) - Q(t) = \frac{t_c}{2} \frac{dQ}{dt} \quad (13)$$

which is solved for $Q(t)$ using an explicit finite difference approach (Overton, 1970). The characteristic time can be determined using either an analytical solution to the kinematic wave equation for smaller watersheds or derived from empirical catchment data (Watt and Chow, 1985). A relationship between the geometry of the catchment and the time it takes a parcel of liquid to travel the length of the catchment (the concentration time, t_c), was derived by Watt and Chow (1985) for large catchment basins (up to 5800 km 2):

$$t_c = 0.128 \left(\frac{L}{S_0^{0.5}} \right)^{0.79} \quad (14)$$

where L is the length from the furthest reach of the catchment to the outlet in km and S_0 is the dimensionless slope of the catchment. In our treatment of overland flow, we use values of L and S_0 from individual catchments in the model topography. As discussed in Section 2.1, catchment lengths in our model topography match those determined from the mapping of channels. While the concentration time is an empirically derived value related to the slope and length of the catchment, the flow time in an open channel is inversely related to the velocity of the flow. Velocity will scale

as the gravitational acceleration over the kinetic viscosity (the dynamic viscosity (μ) over the density (ρ)), thus flow time is proportional to $\mu/\rho g$. Due to the lower gravitational acceleration (g) of Titan and the lower density and viscosity of liquid methane (μ), the time that methane takes to traverse a catchment on Titan should be longer than the time for water to traverse an identical catchment on Earth. For Titan, we scale the concentration time for Earth as:

$$t_{c_Titan} = t_{c_Earth} \left(\frac{g_{Earth}}{g_{Titan}} \right) \left(\frac{\rho_{water}}{\rho_{methane}} \right) \left(\frac{\mu_{methane}}{\mu_{water}} \right) \quad (15)$$

which yields a factor of 3.23. The treatment of overland flow results in a slight lag between the peak precipitation and peak discharge into lakes for the largest catchments. This is included in the models for the sake of completeness, but does not have a significant effect on the results.

While surface liquid was not explicitly channelized in the model, the spatial patterns of overland flow were calculated using an eight-point routing method (Wang and Helmfelt, 1998) in order to determine the size, geometry, and outflow pattern of basins. This method determines surface flow direction at a particular cell based on the steepest downhill slope in the eight surrounding cells. For the catchment scale models, the fractal nature of the synthetic topography resulted in catchment basins with total catchment areas ranging from 27 km² to over 2000 km² with an average of 389 km². Lengths scales of these basins, calculated from basin mouth to divide, ranged from < 10 km to 57 km with an average of 19 km. Polar scale models had total catchment areas ranging from 62 km² to 5200 km² and lengths ranging from < 10 km to 115 km.

Observed fluvial dissection on Titan ranges in spatial extent from the submeter scale (Perron et al., 2006), as observed during the Huygens probe decent, to > 1000 km (Burr et al. 2013). The majority of identified channels having lengths less than 50 km (Langhans et al., 2012), although this estimate is likely underestimated due to the lack of coverage. Channels measured in another study yield a mean length of ~230 km and median length of 155 km for valleys pole-ward of 70°N (Burr et al., 2013). Cartwright et al. (2011) mapped several drainage basins feeding large north polar lakes, finding a catchment area between 1760 km² and 2640 km² for at least one mapped basin.

Thus, despite the lack of channels in the synthetic fractal topography, the size distribution of drainage basins in the model is comparable to that observed on Titan. Our fractal topography lacks the long channels observed in some locations on Titan (Langhans et al., 2012; Burr et al., 2013). However, our average basin lengths reflect the entire surface surrounding the pole, while geomorphic studies are likely biased towards the most well-developed and clearly expressed valley systems. The overall low density of networks in imaged areas of the pole suggest large undissected regions, though this may in part be limited by the quality of the data (Burr et al., 2013).

2.6. Lake scheme

Lakes and seas on Earth have a uniform surface elevation (hydraulic head) that fluctuates in time due to influx and outflux. Earth based models (Harbaugh, 2005; Maxwell and Miller, 2005; Fan et al., 2007) typically impose large bodies of water as constant hydraulic head boundaries throughout the model run. Here we are investigating the influence of hydrological properties on the lake area distribution and seasonal lake area change on Titan, and it is important to allow lakes to form naturally and to fluctuate over time. Liquid that ponds on the surface in these models was run through a lake diffusion scheme in order to bring each lake surface to an approximately constant hydraulic head. This lake treatment solved Eq. (4) at lake pixels over multiple iterations for each

iteration of the subsurface model, with the porosity of the free surface liquid set to 100% and a high permeability value of 10⁻⁶ cm². The lake diffusion was only applied to pixels where the methane table was above the surface. Liquid was allowed to diffuse over the surface as needed to allow natural adjustments of the shoreline.

3. Basin-scale model results

We first focus on a set of basin-scale models to explore the effects of the aquifer properties for identical topography and climate. The basin-scale modeling used synthetic fractal topography in a 674 km × 674 km spatial domain (in order to encompass a region twice the size of Ligeia Mare) at a resolution of 5.225 km/pixel with multiple catchment basins feeding a central topographic low (Fig. 4). A set of models was run to investigate the influence of aquifer permeability, with k_0 ranging from 10⁻¹⁰ to 10⁻⁶ cm², runoff and recharge fractions both set at 50%, and a surface porosity of 30% (Freeze and Cherry, 1979). Other model sets were designed to test the sensitivity of the lakes to the fraction of runoff and recharge, the amount of precipitation that will evaporate from the surface prior to runoff and recharge generation, and the porosity of the aquifer. All model sets used the latitudinally-averaged GCM output between 75° and 90°N, for which the Budyko-type model predicts an annual precipitation excess of ~14% of the total precipitation that reaches the surface, distributed as recharge and runoff. The model results were analyzed by looking at the distribution of lakes and hydraulic head in map view, the time evolution of the different fluxes into the lakes over the entire model domain (direct precipitation, direct evaporation, overland flow, and subsurface flow), and the time evolution of the lake area as a fraction of the total area of the model domain.

3.1. Influence of the aquifer permeability on the lake hydrology

The distribution and flow of methane in the subsurface exerts a strong control over the sizes and distribution of lakes on the surface. Thus, the size-frequency distribution of lakes, the hydrological budget of the fluxes in and out of the lakes, and the rate of lake level change all depend on the properties of the aquifer. Permeability can vary over several orders of magnitude, and thus exerts the strongest control over the lake hydrology. We performed a set of simulations with identical surface runoff scaling and climate conditions, but with a permeability that varied from 10⁻⁶ cm² to 10⁻¹⁰ cm². A high permeability aquifer (e.g. 10⁻⁶ cm²) predicts a large lake with an area of 3 × 10⁴ km² to form in the central basin, with small (~10² km²) and intermediate (~10³ km²) lakes scattered at an average distance of 225 km from the central basin where the methane table intersects local topographic lows (Fig. 6a). The methane table in these models follows a strongly diffused representation of the surface topography, primarily intersecting the surface in the central basin and leaving much of the surrounding surface perched high above the methane table. This results in maximum lake depths of ~450 m for the large central lake and lake depths between 150 and 250 m for intermediate and small lakes (Fig. 6b). The central lake depth predicted by the model is approximately 3 times greater than the maximum depth of a single bathymetry profile across Ligeia Mare (Mastrogiuseppe et al., 2014), but does not account for sedimentation within the lake. Due to the fractal nature of the topography, the central lake does not form within a single low depression but instead within a series of small depressions interconnected by shallow necks, resulting in complex lake morphology. The purely fractal nature of the topography also has some influence on the size frequency and depth of the small lakes, which may be influenced by dissolution not represented in the model.

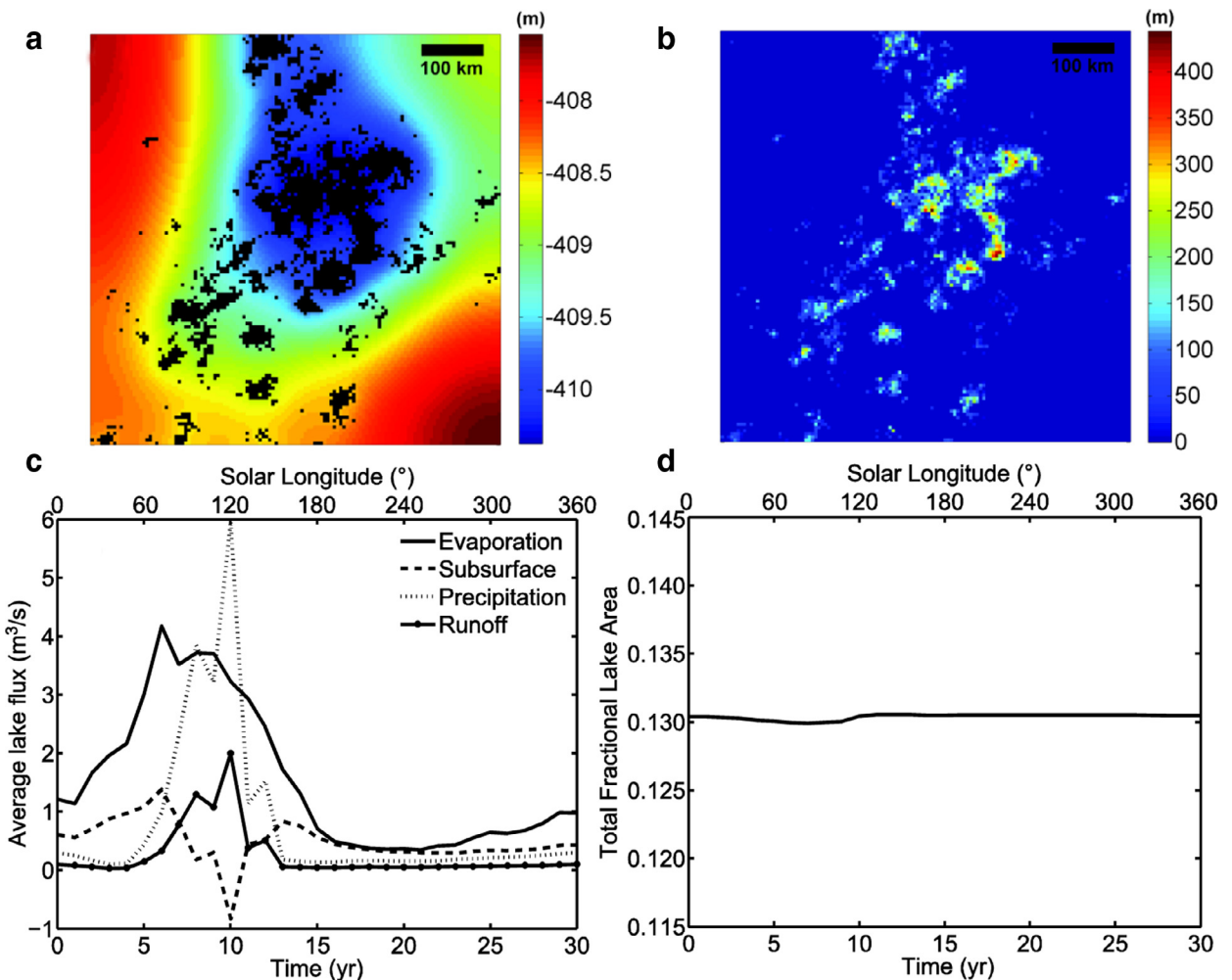


Fig. 6. High permeability model (10^{-6} cm^2) showing the relative hydraulic head with lakes overlain in black (a), the lake depths (b), the average fluxes into (positive precipitation, runoff, and subsurface flow) and out of (positive evaporation and negative subsurface flow) a typical lake over a Titan year (c), and the time evolution of the total lake area as a fraction of the area of the model domain (d). The time evolution in (c) and (d) encompass one Titan year (29.5 Earth years), with spring equinox ($L_s = 0^\circ$) at year 0.

This model also allows us to examine the fluxes of methane into and out of the lakes over the course of a Titan year (Fig. 6c). The volume fluxes in and out of an average lake were calculated by summing the fluxes into all lakes as functions of time and dividing by the total number of lakes. High and variable precipitation rates during the summer months ($L_s \sim 90^\circ$) results in alternating wet and dry periods. During the dry periods, high evaporation from the lake surfaces causes the lake levels to drop below the methane table allowing subsurface flow into the lakes from the surrounding aquifer (Fig. 6c). During times of heavy rainfall and runoff, subtle increases in the lake level relative to the surrounding methane table occur, resulting in periods of net subsurface flow to the surrounding aquifer for the small and intermediate sized lakes. This response from the aquifer mitigates the net liquid lost or gained by the lake from evaporation and precipitation at any given time. The model predicts $< 1\%$ change in lake area as a fraction of the total lake area over a Titan year, which is within the limit of the model resolution (Fig. 6d). The minimal changes in lake area are due to a combination of the approximate balance of fluxes into and out of the lakes, and the large volume of the lakes relative to the fluxes involved. The winter season ($L_s \sim 270^\circ$) is characterized by persistent low precipitation and runoff rates as well as persistently low rates of subsurface flow, with the latter providing the dominant flux into the lake. Lake level change is minimal during this period and subsurface flow is dominated by the central low hydraulic head. The high

permeability of the aquifer results in subsurface flow contributing $65.2 \text{ km}^3/\text{Titan-yr}$ into all lakes in the model domain or 32% of the total inflow (with 17% being sourced from runoff and 51% from direct precipitation onto the lake surfaces).

Similar to the high permeability case, the hydrology of an intermediate permeability aquifer (10^{-8} cm^2) is dominated by a central lake ($\sim 2 \times 10^4 \text{ km}^2$) located in the largest topographic depression (Fig. 7a) with a lake depth of $\sim 400 \text{ m}$ (Fig. 7b). Unlike the high permeability case, at intermediate permeability there is not an instantaneous balance between subsurface flow and the net flux from evaporation, precipitation, and overland flow. Subsurface flow maintains a relatively constant flux into the lakes, while the other fluxes exhibit strong seasonality (Fig. 7c). Nevertheless, there is little seasonal change in lake area since the large sizes of the lakes stabilize them against the comparatively small seasonal variations in net flux (Fig. 7d). Subsurface flow constitutes the primary flux into lakes during the quiescent winter months. Over the course of a year, subsurface flow accounts for $55.8 \text{ km}^3/\text{Titan-yr}$ into all lakes in the model domain or 29% of the total inflow with direct precipitation and runoff accounting for 51% and 20% respectively (Fig. 7c). In contrast to the high permeability case, the intermediate permeability results in an increase in the hydraulic head gradient, forming a greater number of small to intermediate-sized lakes where the methane table intersects the surface at small topographic depressions, while decreasing the size of the large central lake. The

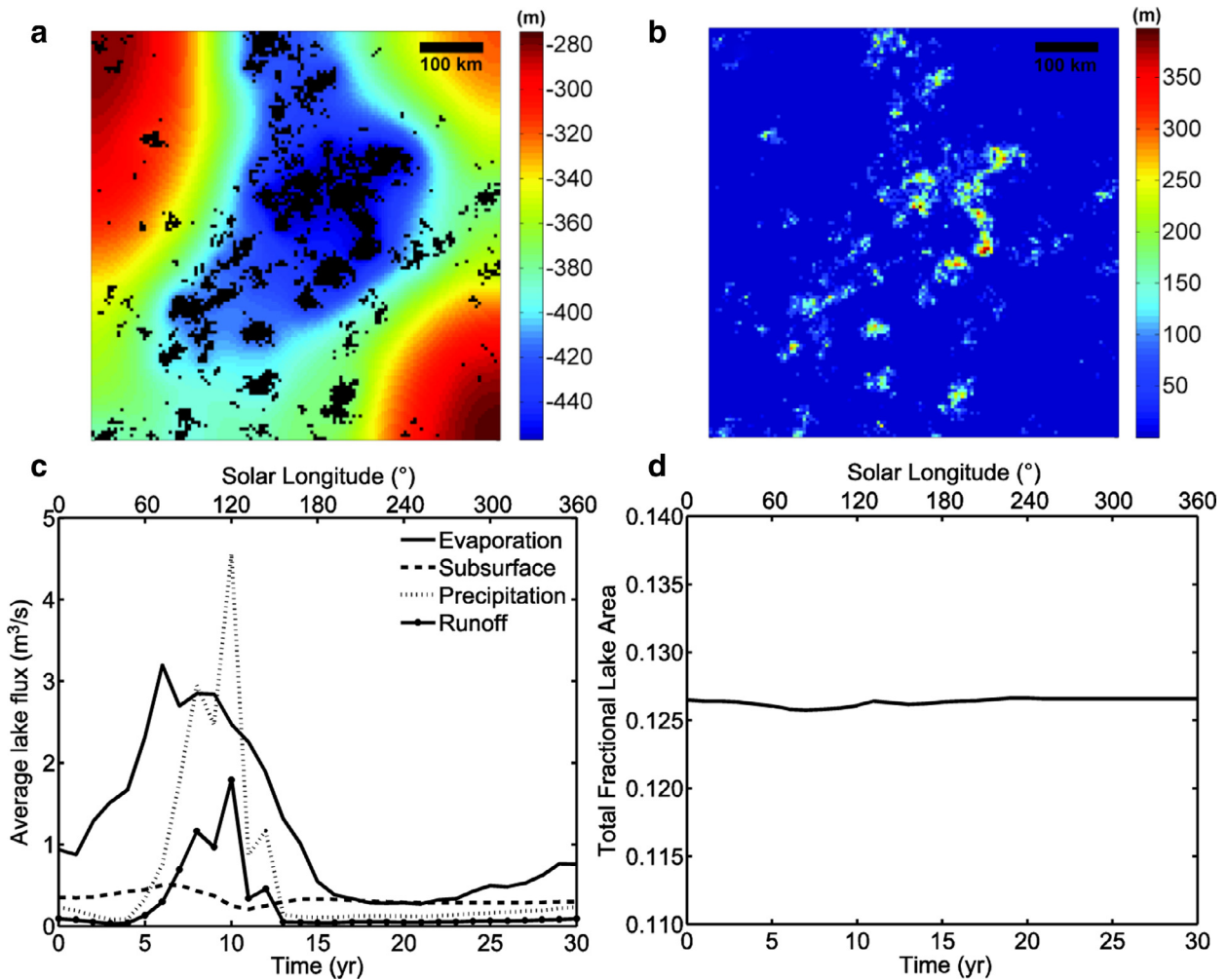


Fig. 7. Intermediate permeability model (10^{-8} cm^2) showing the relative hydraulic head with lakes overlain in black (a), the lake depths (b), the average fluxes into and out of a typical lake over a Titan year (c), and the time evolution of the total lake area as a fraction of the area of the model domain (d).

total lake area is somewhat reduced relative to the high permeability case, largely as a result of evaporation from the methane table where it approaches the surface, which occurs more widely at lower permeability.

In contrast to the previous models, low permeability aquifers (10^{-10} cm^2) constrict flow through the aquifer raising the methane table close to the surface throughout the model domain. This prevents large lakes from forming in the deepest basin and limits the size of the largest lake to 850 km^2 (Fig. 8a), which is only $\sim 3\%$ of the size of the largest lake in the high permeability model. Small lakes are now favored within small local topographic basins throughout the model domain with an average lake depth of $\sim 40 \text{ m}$ (Fig. 8b). The predicted subsurface flux shows little change over the course of a Titan year and is dominated by short flow paths to local topographic lows. The subsurface flux into lakes is reduced relative to the high permeability case ($27.2 \text{ km}^3/\text{Titan-yr}$ or 16% of the total inflow to the lakes), increasing the fractional input from runoff (33% of the total inflow) and direct precipitation (51% of the total inflow) (Fig. 8c). The contribution from subsurface flow does not scale directly with the permeability because of the much greater hydraulic gradients at low permeability. The smaller size of the lakes compared to the high and intermediate permeability cases results in greater sensitivity of the lakes to variations in evaporation and precipitation, and larger seasonal changes in lake area. The total fractional lake area ranges from 10.8% to 12.8% of the total model area (Fig. 8d), amounting to a $\sim 16\%$ variation

in the lake area as a fraction of the total lake area over a Titan year. A large increase in lake area is predicted to occur in mid to late northern winter as the evaporation rate from the lake surface decreases.

3.2. Sensitivity to other parameters

We examined a wide range of parameter space in all of the terms that affect the hydrology, finding that most have only a second-order effect on the results. The assumed porosity controls the storativity of the aquifer, and thus the time-dependent response of the aquifer to any applied forcing. Substantially reduced porosity (5% surface porosity) results in a larger seasonal change in lake area, but does not otherwise change the model predictions.

The assumed Budyko relationship determines what fraction of the precipitation is available for hydrological activity as either runoff or recharge, rather than directly evaporating from the surface. However, the partitioning of this fluid into runoff and recharge is poorly constrained given the unknown nature of Titan's surface materials and the poorly constrained interaction of liquid methane with the ice-organic mixture that likely comprises the soil. The amount of runoff compared to recharge to the aquifer affects the timing of lake level change over a Titan year, thus influencing the seasonal changes in lake area. Surface runoff acts as a rapid mechanism for influx into the lakes that closely follows the temporal distribution of precipitation, while recharge to the

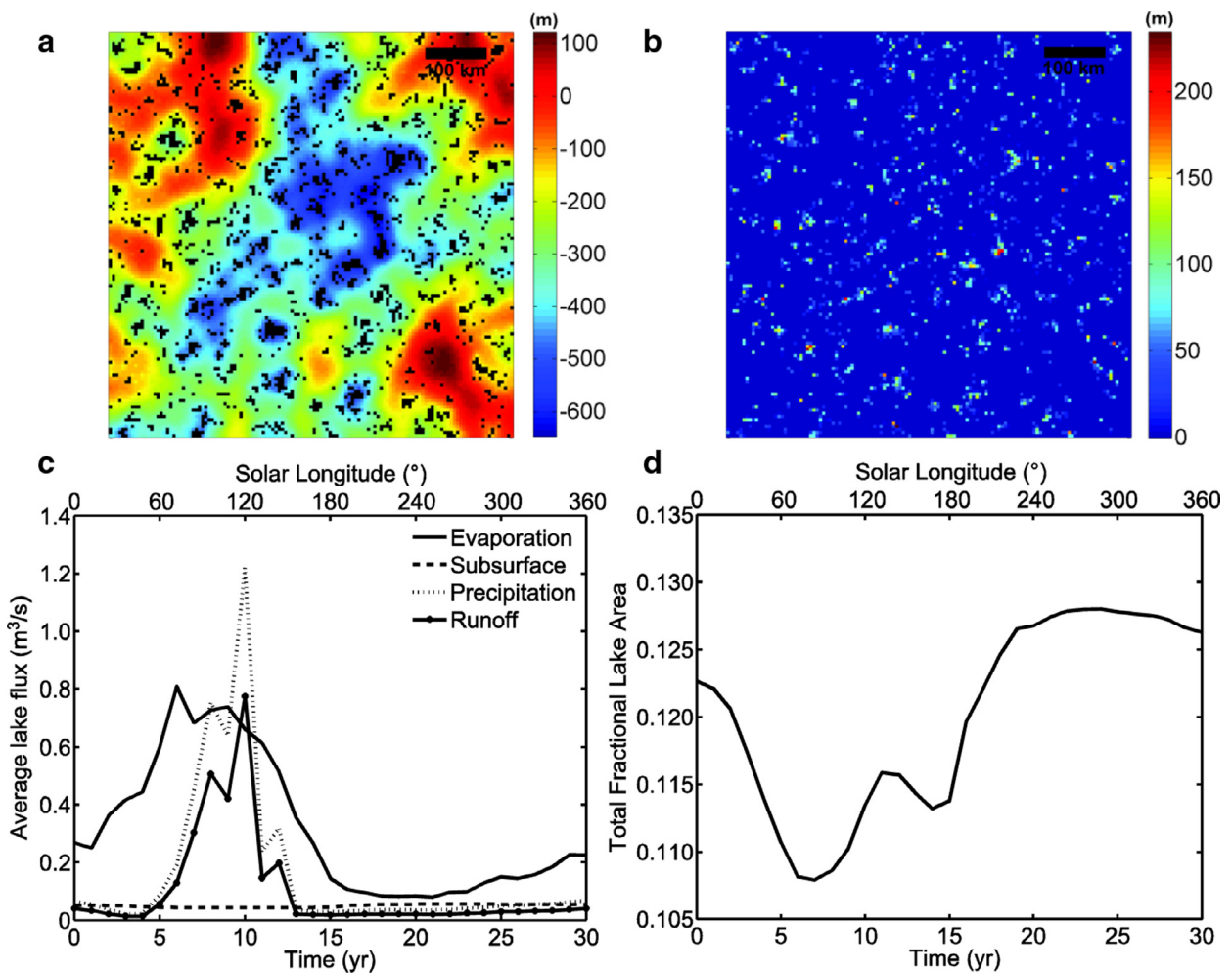


Fig. 8. Results for models with a low permeability (10^{-10} cm^2) showing the relative hydraulic head with lakes overlain in black (a), the lake depth map (b), the average fluxes into and out of a typical lake over a Titan year (c), and the total fractional lake area change over the course of a Titan year (d).

aquifer determines the volume of methane available for slow influx to the lakes by subsurface flow. For intermediate to high permeability aquifers, increasing either the runoff or recharge fractions to 100% of the excess precipitation has little effect on the results due to the high rates of subsurface flow in these aquifers. For the case of 100% runoff, the runoff ponds in the closest topographic depression where it infiltrates and contributes to subsurface flow, resulting in only a minor redistribution of surface fluid prior to infiltration. For low permeability aquifers, increasing the recharge fraction to 100% of the excess precipitation results in a decrease in the total lake area and a large seasonal lake area change. In this case, the aquifer recharge is inefficiently removed by subsurface flow resulting in a rise in the methane table toward the surface, where methane can be lost to evaporation. As a result of the increased evaporation from the methane table, the total lake area is reduced.

There is also significant uncertainty in the fraction of the precipitation that will evaporate directly from the surface prior to generating runoff or aquifer recharge (the applied Budyko relationship). The Earth-based Budyko relationship allows 14% of the precipitation to generate runoff and recharge. The lack of plant cover on Titan in comparison to Earth may reduce the tendency to store liquid in the near-surface soil layer, and thus reduce the fraction of the precipitation that is subject to direct evaporation from the soil layer. We tested this with a model in which no Budyko scaling was applied, thus allowing all precipitation to generate ei-

ther runoff or aquifer recharge. This has the effect of significantly increasing the lake area for all models. Scaling the Budyko relationship to allow ~46% of the GCM predicted precipitation to either runoff or recharge produces a Ligeia Mare-sized lake for a high permeability aquifer, suggesting that the Earth-based relationship may underestimate recharge and runoff on Titan. However, this does not alter the fundamental conclusions regarding the role of permeability in controlling the balance between small to intermediate size lakes and large seas.

4. Polar model results

The previous basin-scale hydrological models described above gave insight into the general behavior of hydrology on Titan, but focused on an isolated basin influenced by an average GCM output over the latitudes at which lakes are observed. Large basins on Titan can span a range of latitudes (e.g. Kraken Mare) and may be influenced by differing climates at different latitudes. Furthermore, flow both within the lakes (Lorenz, 2014) and in the subsurface from more temperate high latitudes to more arid low latitudes may significantly affect the hydrology. By using the GCM output to spatially vary the precipitation and evaporation potential values over a larger model domain representing the entire north polar region, we were able to investigate the importance of the latitudinal variation in climate and long-distance subsurface latitudinal transport on the latitudinal distribution of lakes (Fig. 9a). The polar model

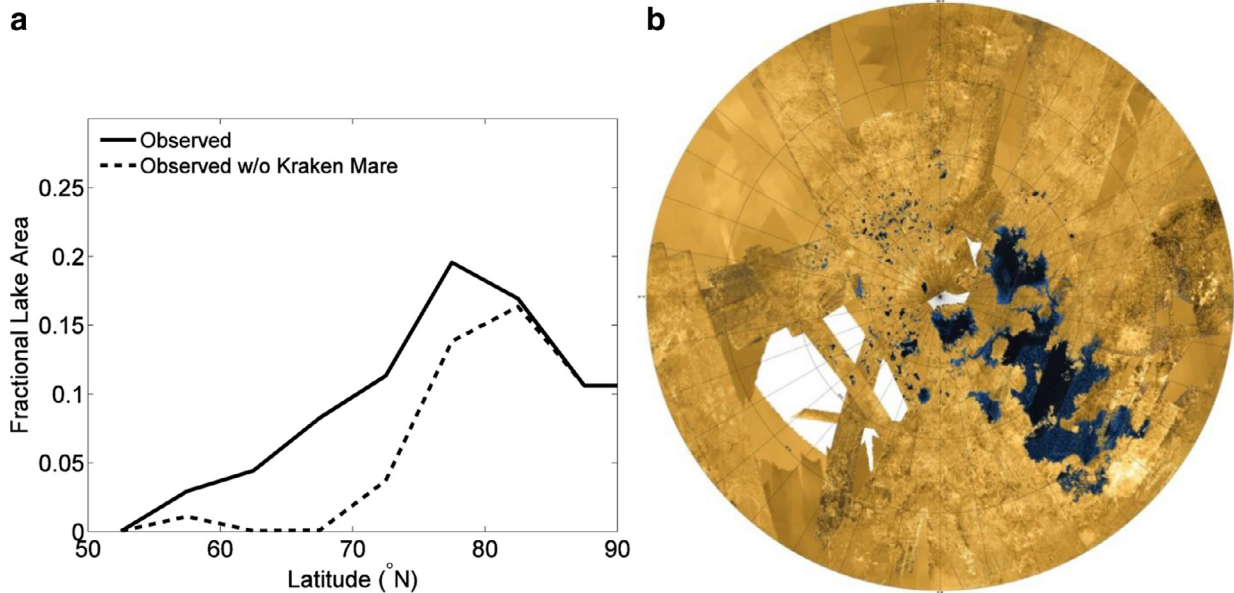


Fig. 9. The distribution of the fractional lake area (expressed as a percentage of the total surface area) as a function of latitude observed at the north polar region (a), with (solid) and without (dashed) Kraken Mare. The observed lake distribution was calculated from a SAR image mosaic over the north polar region down to 50°N (b; image credit: NASA/JPL-Caltech/ASI/USGS, <http://photojournal.jpl.nasa.gov/catalog/PIA17655>).

was also used to investigate the effects of decreased evaporation over large polar seas due to either accumulated ethane or other solutes (Lorenz, 2014) or to lake effect changes to the local climate (Tokano, 2009). This was implemented in the hydrological model by simply decreasing the evaporation potential over Kraken Mare and increasing the total amount of aquifer recharge and surface runoff at the high polar latitudes. The possible effects of a non-uniform permeability distribution at the north polar region was also investigated by varying the permeability with latitude as supported by evidence for karst at high polar latitudes (Mitchell et al., 2008; Cornet et al., 2015).

The polar model encompassed the north polar region down to 45°N, in a 4000 km × 4000 km domain (Fig. 9b). The model used a flat circular domain rather than a curved spherical cap for simplicity. This has the effect of slightly overestimating the divergence of subsurface flow from high to low latitudes, and thus slightly underestimating the local flux at lower polar latitudes. However, since the hydrological processes of interest dominantly occur at latitudes above 75°N and at the transition to more arid climates at 75°N, this simplified geometry has little effect. For the simple case of a constant volumetric flow of methane from high to low latitudes, the assumed flat model domain decreases the local flux per unit distance crossing 75°N by only 1% relative to what a spherical cap model would predict. This model used synthetic topography generated from a modified fractal scheme so as to capture the long wavelength nature of the topography around the pole and impose basins for the largest seas, as discussed in Section 2.1. With this topographic model, the conditions needed to form both the large seas, in particular Kraken Mare, and the distribution of smaller lakes can be investigated. The GCM inputs to the hydrological model were spatially distributed in 5° latitude increments in a polar geometry. The lake area as a function of latitude was compared to the observed lake area distribution over the same north polar region with and without Titan's largest sea, Kraken Mare (Fig. 9a). The removal of Kraken Mare from the observed lake distribution allows for the comparison of the distribution of the smaller lakes with the distribution predicted by the models, as Kraken Mare dominates the north polar lake area.

4.1. Influence of aquifer properties on the latitudinal distribution of lakes

Based on the results of the basin-scale models, we here consider only the high and intermediate permeability cases. The low permeability models at the basin-scale predicted many small lakes perched at high elevations, and large seasonal variation in lake area, both in conflict with observations. A high permeability aquifer (10^{-6} cm^2) throughout the model domain allows significant subsurface flow from the pole to mid-latitudes due to a precipitation-induced latitudinal hydraulic head gradient. High precipitation rates at latitudes $> 75^\circ\text{N}$ generate aquifer recharge and an elevated hydraulic head relative to the more arid lower polar latitudes (Fig. 10a), resulting in a net loss of methane from the higher latitudes by subsurface flow to low latitude sinks. The north polar hydrology in this high permeability case is controlled by topographic depressions at low latitudes, primarily the Kraken Mare basin and a low topographic region located at 50°N in the SAR topography (Fig. 4a) that forms a basin between 40°N and 50°N in the synthetic fractal topography (Fig. 4b). This topographic low is observed in the SAR topography and is associated with the Ganesha Macula region. While initial studies suggested a cryovolcanic origin for Ganesha Macula (Lopes et al., 2007), recent studies have found that the low topography and morphology are more consistent with an origin through hydrological and fluvial processes (Le Gall et al., 2010; Lopes et al., 2013). While some lake formation is predicted below 75°N, the high aridity at lower polar latitudes only allows a few small lakes to form and the total lake area at all latitudes predicted by this model is significantly less than the observed lake area (Fig. 11a). The low total lake area in the north polar region, predicted by the high permeability model, is a result of the efficient movement of methane out of the wet high latitudes to the arid regions at lower polar latitudes. This efficient equator-ward transport of methane results in a nearly flat methane table, with only $\sim 150 \text{ m}$ variation in hydraulic head from the pole to low latitudes, leading to a methane table deep beneath the surface over most of the model domain.

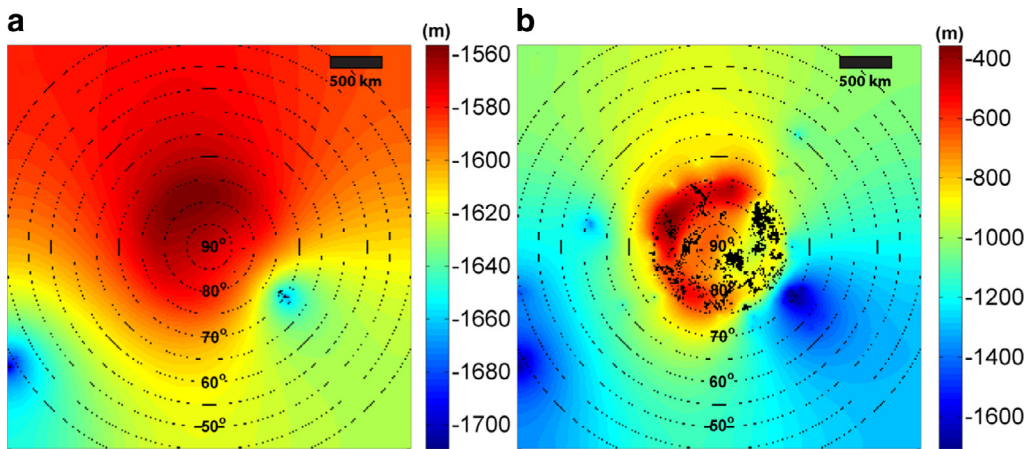


Fig. 10. Hydraulic head maps with lakes overlain in black for the polar models with a permeability of 10^{-6} cm^2 (a) and 10^{-8} cm^2 (b).

At intermediate permeability (10^{-8} cm^2), comparable to an unfractured sandstone or a fractured granite aquifer on Earth, the polar model predicts that the vast majority of methane ponded on the surface would be contained at latitudes $> 75^\circ\text{N}$ (Fig. 10b). High rates of precipitation at latitudes $> 75^\circ\text{N}$ again cause a climate-induced hydraulic head gradient from the pole to the mid-latitudes, driving equator-ward flow in the subsurface. However, the permeability in this case is too low to allow sufficient subsurface flow to permit substantial lake formation at more arid latitudes below 75°N . At higher latitudes, the increased hydraulic head and reduced subsurface flow towards the mid-latitudes results in the formation of small lakes and seas within the Ligeia Mare and Punga Mare basins, but the model does not produce large seas comparable to those observed. Although inter-latitudinal flow allows some lakes to form at lower polar latitudes in the Kraken Mare basin, the predicted latitudinal distribution of lakes for this intermediate permeability aquifer is strongly focused around the pole and does not match the latitudinal distribution of lakes below 75°N , even if Kraken Mare is excluded from the observed distribution (Fig. 11a).

4.2. Influence of increased runoff and aquifer recharge

Both the high and intermediate permeability polar models fail to match the lake area distribution and to generate a Kraken-sized sea due to the high evaporation potential at the lower latitudes reaches of the Kraken Mare basin. This suggests that the Budyko-type method used in the models may be underestimating the aquifer recharge and runoff generated by the precipitation. While the observed manifestations of hydrologic activity on Titan such as fluvial dissection, storms, and lake morphology appear similar to their counterparts on Earth, both the solid and liquid materials involved in the hydrology are very different. Based on the complex nature of hydrocarbons in the atmosphere, at the surface and potentially in the subsurface, one might expect significant departures from processes on Earth. Particularly, the interaction of liquid hydrocarbons with solid hydrocarbons and ice is poorly understood, and may be a key process in determining the amount of methane that recharges the aquifer or generates runoff, rather than evaporating immediately back into the atmosphere. Increased runoff and aquifer recharge might arise due to either the effects of an organic-rich “regolith” layer on Titan or enhanced recharge due to the wetting behavior of liquid methane on crystalline ice (Sotin et al., 2009).

A model with no Budyko-scaling was used in order to test an endmember scenario in which all of the methane that falls on the surface will either recharge the aquifer or runoff over the surface,

with no direct evaporation of precipitation back into the atmosphere. The increased recharge to the aquifer and surface runoff raises the methane table at the high latitude polar regions, filling the Ligeia Mare and Punga Mare basins while equatorward subsurface flow reaches the Kraken Mare basin forming a small sea. As found in the previous high permeability case, the observed lake distribution is strongly underpredicted in this model (Fig. 11b) and a Kraken-sized sea cannot form due to the high evaporation potential over the Kraken Mare basin. At the high polar latitudes, the lake area agrees with the observed lake area due to the filling of Punga Mare and Ligeia Mare, but the abundant small lakes observed extending down to 70°N are not predicted.

For the intermediate permeability case, increased recharge and runoff increases the total lake area at high polar latitudes, but inefficient subsurface flow still prevents substantial lake formation below 75°N (Fig. 12b). Lake formation below 75°N is confined to the Kraken Mare and Jingpo Mare basins, though only small lakes form in these basins. The high polar latitudes are nearly saturated in this model, over-filling Ligeia and Punga Mare, and forming numerous other intermediate to large sized lakes that cover the majority of the high polar latitudes down to 75°N . The latitudinal distribution of lakes is significantly overpredicted at high polar latitudes and underpredicted at lower polar latitudes (Fig. 11b). Thus, both models without Budyko-scaling, allowing all of the precipitation predicted by the GCM to generate runoff and recharge to the aquifer, still fail to predict the observed latitudinal lake distribution and to form a Kraken-sized sea within the imposed Kraken Mare basin.

4.3. Influence of decreased evaporation over Kraken Mare

The previous models showed that hyper-arid conditions at latitudes below 75°N prevent a large Kraken-sized sea from forming. One possible solution to this problem is that the evaporation rate over Kraken Mare may be lower than the values predicted by the general circulation model. At temperatures on Titan, the volatility of ethane is much lower than that of methane due to low ethane saturation pressure (Lunine et al., 1983; Aharonson et al. 2009), suggesting that the evaporation of ethane is insignificant on seasonal Titan timescales. Tokano (2009) found that 83% of ethane or other organic solutes within large seas at Titan's north polar regions will inhibit the evaporation of methane, while seas with greater amounts of methane will contribute to elevated atmospheric methane humidity and fluctuating evaporation rates. These results suggest that higher concentrations of ethane or other organic solutes within the large seas will greatly reduce the evaporation rate of methane. This effect was used to estimate the amount of ethane or organic

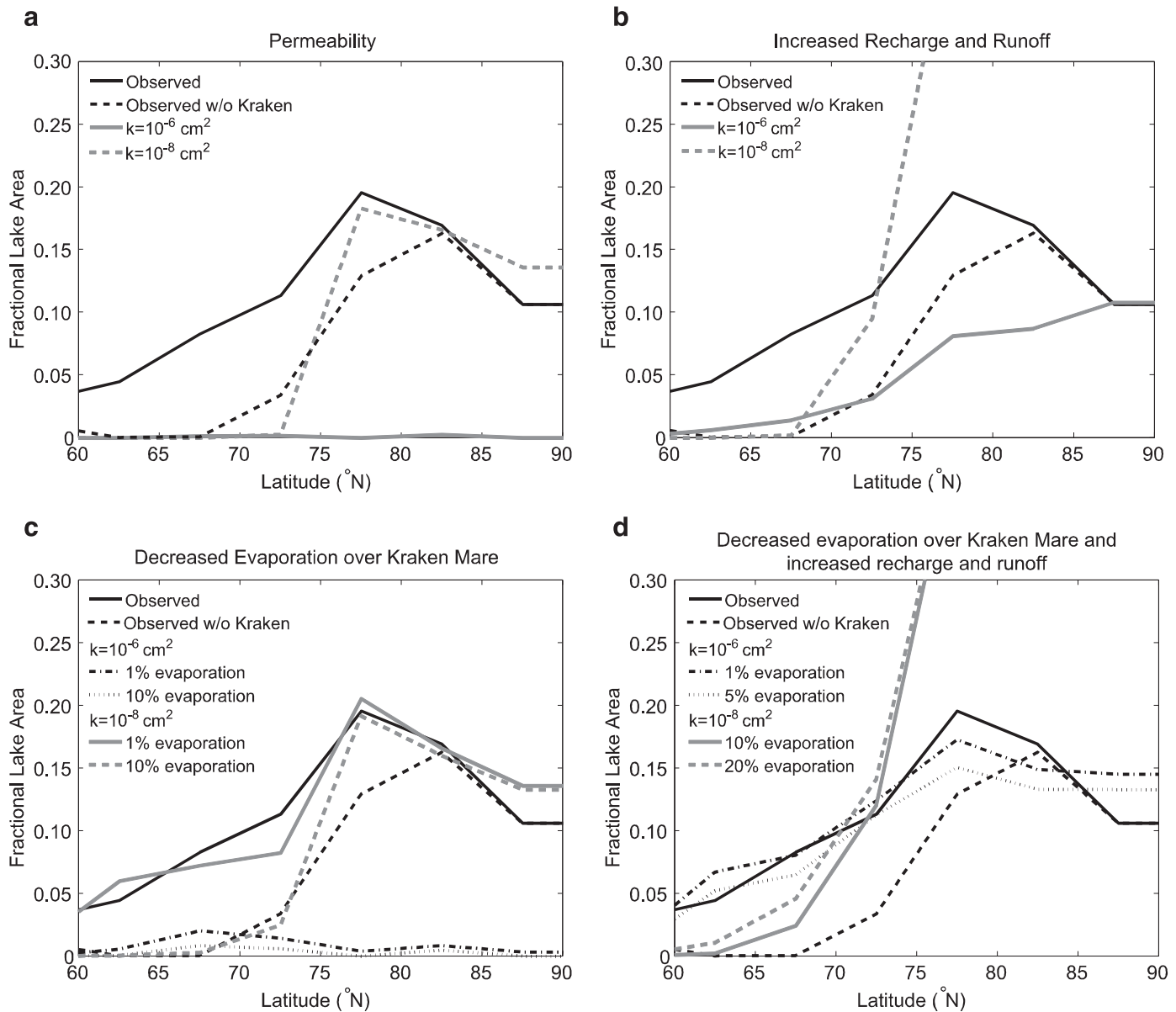


Fig. 11. Predicted lake area as a function of latitude showing the effect of permeability (a), increased runoff and recharge (b), applying a factor to decrease the evaporation over Kraken Mare (c), and increasing the runoff and recharge while also scaling the evaporation over Kraken Mare (d).

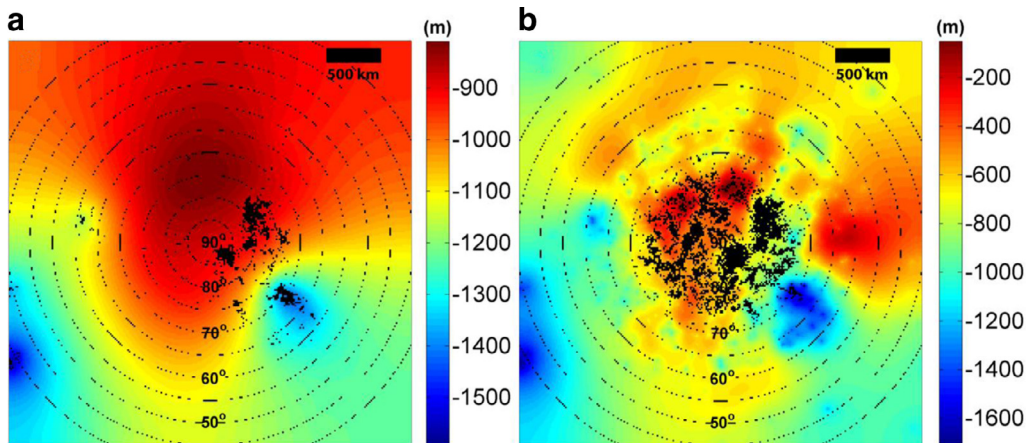


Fig. 12. Results from the polar models showing hydraulic head maps with lakes overlain in black for a permeability of 10^{-6} cm^2 (a) and 10^{-8} cm^2 (b) with increased runoff and recharge.

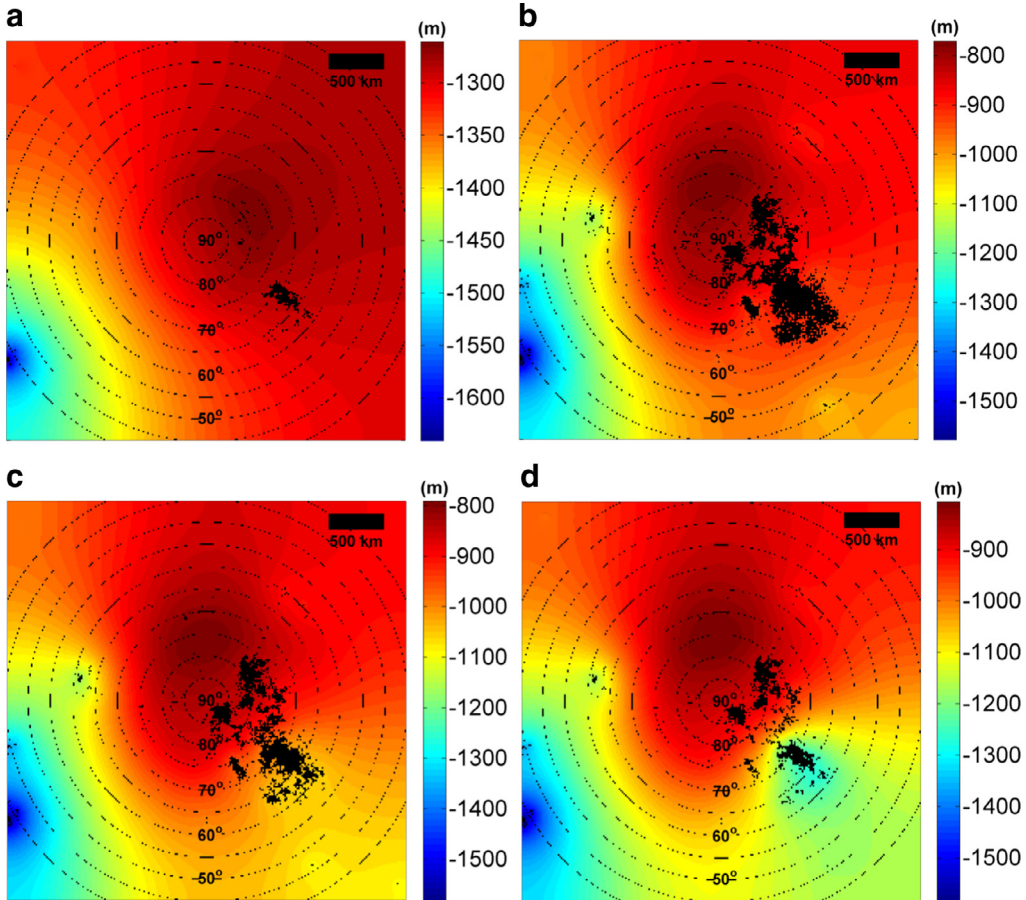


Fig. 13. Polar model results showing hydraulic head maps for a high permeability case with 1% evaporation scaling over Kraken Mare (a), 1% evaporation scaling over Kraken Mare and increased runoff and recharge (b), 10% evaporation scaling over Kraken Mare and increased runoff and recharge (c), and 40% evaporation scaling over Kraken Mare and increased runoff and recharge (d).

solutes within Kraken Mare based on a mass balance within the Ligeia and Kraken Mare basins (Lorenz, 2014). Using a direct scaling of the evaporation with the organic solute concentration, that study found the involatile concentration within Kraken Mare to be ~60%, reaching greater values at lower latitudes. Other work has suggested that the composition of Titan's largest seas are close to vapor equilibrium with the atmosphere (Mastrogiuseppe et al., 2014), which will also act to greatly reducing the evaporation from the large seas. Evaporative cooling over large bodies of liquid will also suppress the evaporation rate over Kraken Mare. The evaporation potential output by the GCM used in this work predicted high rates of evaporation potential at lower polar latitudes. However, the lack of surface methane at lower polar latitudes in the GCM produces a higher evaporation rate than if surface methane were present, due to latent heat effects as evaporation occurs. Here, we tested this effect by applying a constant scaling factor to the evaporation potential over lakes and seas within the Kraken Mare basin, with scaling factors ranging from 0.01 to 0.2. This scaling tests the net effect of evaporation suppression due to both a lake effect on the climate and the effects of the concentration of ethane or organic solutes within Kraken Mare.

We also tested a variable scaling of the evaporation rate over Kraken Mare, based on the model-predicted changes in the methane-solute ratio within the sea. In this approach, we initialized the model with a Kraken Mare with an assumed involatile volume, and let the involatile fraction evolve with time in response to the fluxes of methane into and out of the lake. These models generated similar results to the models with constant scaling of

the evaporation over Kraken, and thus we focus our discussion below on the simpler models with the constant scaling factors.

At high permeabilities (10^{-6} cm^2), a decrease in the evaporation potential over Kraken Mare to 1% of the evaporation rate predicted by the GCM results in a larger lake forming within the Kraken basin relative to the previous high permeability case (Fig. 13a), but the total lake area and the size of the lake in the Kraken Mare basin are still much smaller than the observed lake areas (Fig. 11c). In this model, the high rate of subsurface flow in a high permeability aquifer flushes liquid out of the Kraken Mare basin toward other small but low elevation depressions in the arid low latitudes. Similar to the previous high permeability case, the rapid removal of methane from the polar region inhibits lake formation at the higher polar latitudes, thus the primary methane sink is evaporation from small lakes and saturated surfaces at the dryer low latitudes. In this model, the suppression of evaporation over the Kraken Mare basin reduces its role in removing methane from the system to balance the precipitation and aquifer recharge at the high polar latitudes. A topographic low at a separate low latitude basin between 40°N and 50°N instead becomes the dominant sink for the system and controls the flow of methane in the subsurface (Fig. 13a).

A high permeability model with an evaporation scaling factor of 1% over Kraken Mare, while also allowing all precipitation to either runoff or recharge the aquifer (i.e., no Budyko scaling of the precipitation), produces a lake distribution similar to the observed lake distribution (Fig. 11d) and allows a Kraken-sized sea to form (Fig. 13b). This model is dominated by large seas in the

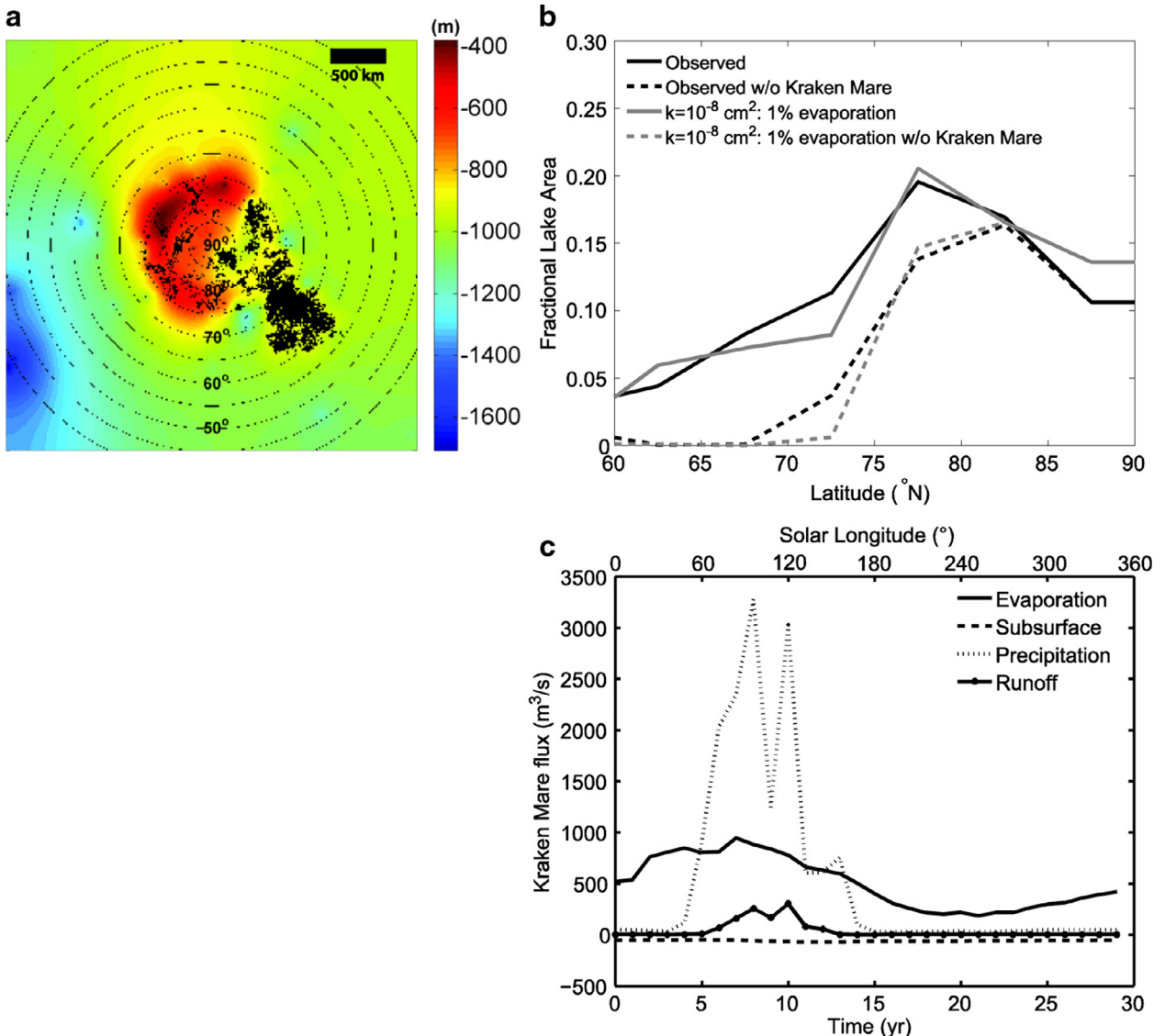


Fig. 14. The hydraulic head map (a) for the intermediate permeability polar model with a 1% evaporation scaling factor over Kraken Mare. The lake distribution as a function of latitude compared to the observed lake distribution is shown in (b), and the hydrological budget of Kraken Mare over the course of a Titan year is shown (c).

north polar regions filling the Ligeia Mare, Punga Mare, Jingpo Lacus, and Kraken Mare basins, but does not predict the large number of smaller lakes that are observed at other longitudes. While this model does fit with the observed latitudinal lake distribution, the requirement for all of the precipitation to runoff or recharge the aquifer is unrealistic, and the lack of small lakes is in contrast with the observed lake distribution making this model less than ideal. When the evaporation over Kraken Mare is scaled by a factor of 0.1 (Fig. 13c) or 0.4 (Fig. 13d) in models with increased runoff and recharge, a lake smaller than Kraken Mare is predicted to form within the Kraken Mare basin. This suggests that, even with increased recharge and runoff in the system, a small evaporation scaling factor (~1%) is needed to form a Kraken-sized sea at high permeability values, and the models still fail to predict the distribution of smaller lakes.

In the case of the intermediate permeability aquifer with a 1% evaporation scaling over Kraken Mare, a large Kraken-sized sea forms in the Kraken Mare basin (Fig. 14a). The latitudinal lake distribution predicted by this model agrees with the observed lake distribution (Fig. 14b). This model predicts Ligeia Mare and Punga Mare-sized lakes at the high polar latitudes, and smaller lakes

down to 75°N, but lacks small lakes between 70°N and 75°N and fails to predict a fully filled Jingpo Lacus basin. Fluid sourced from subsurface flow, direct precipitation, and runoff from the high polar latitudes remains in the Kraken Mare basin as the decreased rate of subsurface flow from the basin relative to the high permeability case and the reduced evaporation inefficiently remove fluid from the lake (Fig. 14c). Subsurface flow acts as a net sink from Kraken Mare as a whole, though this reflects the balance of flow into the lake at high latitudes and away from the lake at low latitudes. With the exception of Kraken Mare, dry conditions below 75°N and a lack of subsurface flow prevents stable lake formation at low latitudes. At the lowest topographic depressions below 75°N, the methane table lies incident with the surface, but the high evaporation potential at these latitudes prevents methane from ponding.

Similar to the previous high permeability model, any increase in the evaporation potential over Kraken Mare prevents a Kraken-sized sea from forming (Fig. 15a). Intermediate permeability models with high recharge and runoff and applying 1% scaling to the evaporation potential over Kraken Mare greatly overestimate the abundance of lakes at high latitudes (results not shown). Models

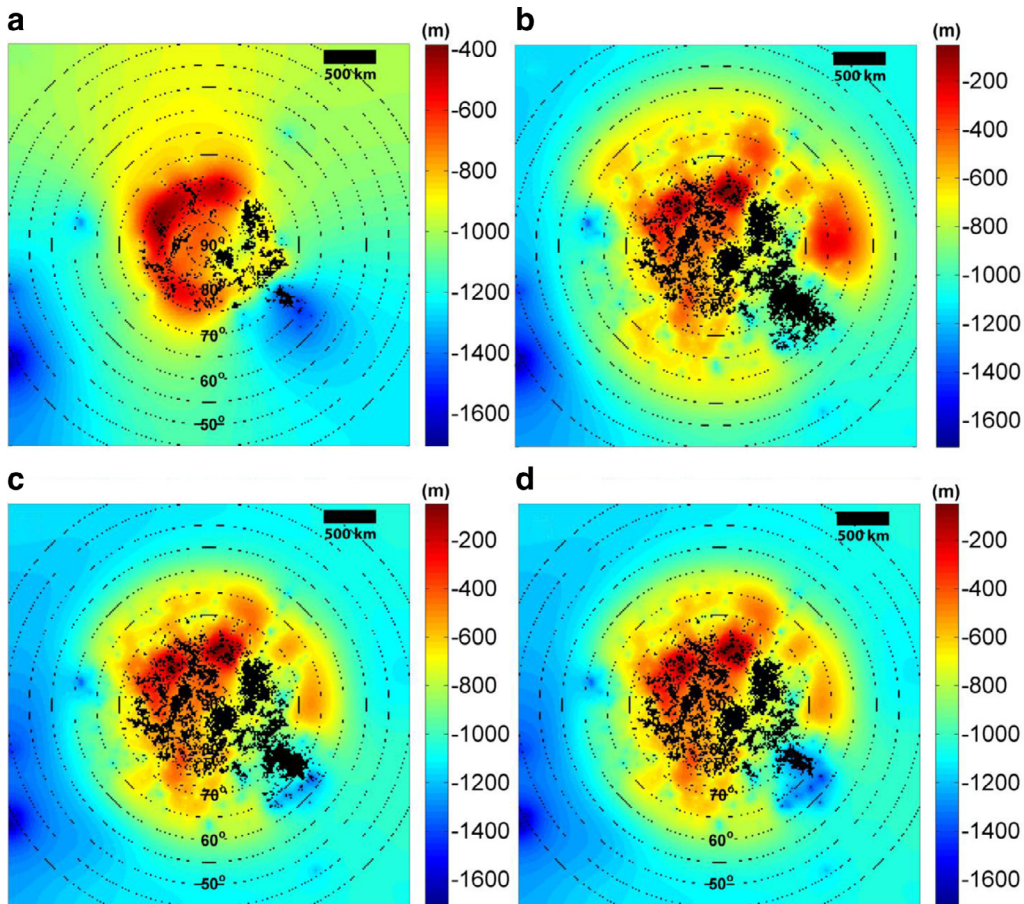


Fig. 15. Polar model results showing hydraulic head maps for an intermediate permeability case with 5% evaporation scaling over Kraken Mare (a), 5% evaporation scaling over Kraken Mare and increased runoff and recharge (b), 10% evaporation scaling over Kraken Mare and increased runoff and recharge (c), and 20% evaporation scaling over Kraken Mare and increased runoff and recharge (d).

with high recharge and runoff with 5%, 10%, and 20% scaling of the evaporation potential over Kraken Mare also overpredict lake formation at the high polar latitudes and fail to form a sufficiently large sea within the Kraken Mare basin (Fig. 15b-d).

4.4. Influence of a non-uniform permeability distribution around the north pole

The models above assumed a laterally uniform permeability distribution in the model domain but this may not be the case at the north polar region. Recent observations of the north polar region with Cassini's Imaging Science Subsystem (ISS) found a bright region at ISS wavelengths encompassing the northern lakes with a drop off in albedo at lower latitudes (Turtle et al., 2013). This suggests that the surface material at the north polar region differs from surface material at the mid-latitudes. The aquifers in the north polar region may contain soluble organic fallout material (Lavvas et al., 2008; Krasnopolsky, 2009). The presence of morphologies consistent with karst features near the polar regions (Mitchell et al., 2008) suggests that the permeability at the north polar region may be higher than that over the majority of Titan as a result of dissolution in the subsurface (Malaska and Hodys, 2014). For karst systems on Earth, the permeability and subsurface conduit system is controlled by the regional climate, with wetter climates forming larger interconnected cave systems and drier climates inhibiting cave formation (Webb and James, 2006). The majority of rainfall that reaches the surface on Titan occurs at latitudes above 75°N, which may contribute to a more developed, higher permeability aquifer around the north polar region. Small-

scale conduits and fractures in poorly developed karst aquifers will increase the average permeability of the aquifer but can still be approximated by Darcy flow in the subsurface. In contrast, large cave systems found in mature carbonate aquifers on Earth act as subsurface fluvial systems with dimensions comparable to the individual catchment basins on Titan (e.g., Mammoth cave has a total length of cave passages of over 600 km in a catchment with an area of ~200 km²). Flow through such a large-scale cave system will behave similar to the overland flow and not affect the model results significantly. However, the overall increase in permeability in karstic aquifers may affect flow in the north polar region.

In order to approximate variations in permeability due to karst at the north polar region, we vary permeability from higher permeability (10^{-7} cm²) between 75° and 90°N to an intermediate permeability (10^{-8} cm²) below 75°N. Higher permeability around the pole should result in a better match to the sizes and distributions of high latitudes lakes, while the intermediate permeability at low latitudes will prevent rapid southward flow and loss of methane at arid low latitudes. Based on the results of a parameter sensitivity investigation, a scaled Budyko-type method was used, allowing approximately three times as much methane to generate runoff and recharge compared to the nominal models. The evaporation potential predicted by the GCM over Kraken Mare was scaled by a factor of 0.01. While other non-uniform permeability models with different choices for the permeabilities, recharge and runoff fractions, and evaporation decrease over Kraken Mare were investigated (results not shown), this model was chosen based on a qualitative and quantitative

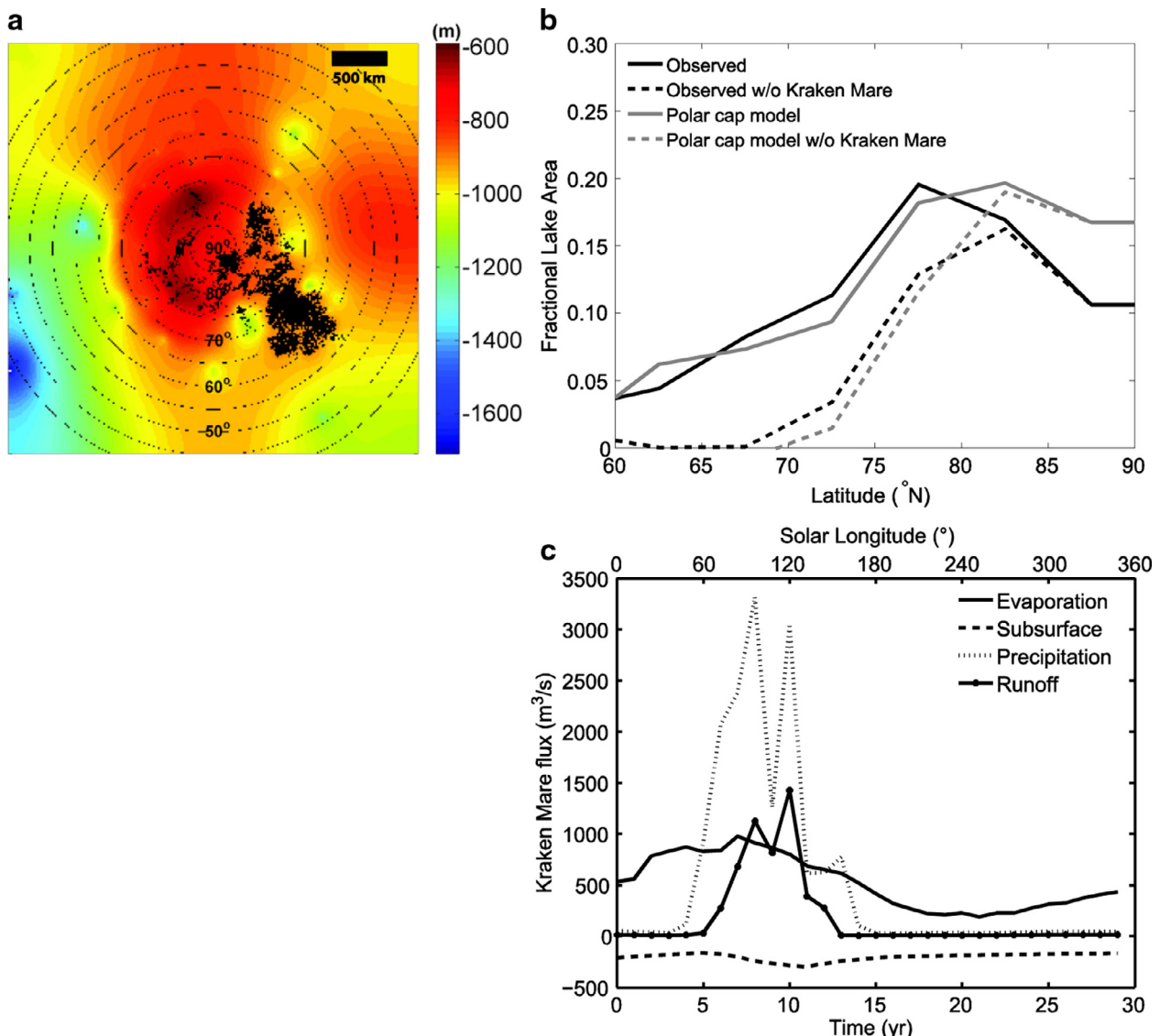


Fig. 16. The hydraulic head map (a) for the polar cap model with a 1% evaporation scaling factor over Kraken Mare and allowing 30% of the precipitation to reach the surface/subsurface hydrology. The lake distribution compared to the observed lake distribution (b) and the hydrology of Kraken Mare is shown (c).

comparison with the observed lake distribution at the north polar region.

For the non-uniform permeability model, the lower permeability below 75°N restricts flow to the arid lower polar latitudes, causing increased hydraulic head above 75°N relative to the uniform permeability models (Fig. 16a). This allows more lakes to form at latitudes above 75°N as liquid encroaches the surface at higher elevation, forming small lakes at the high polar latitudes down to 70°N and filling the Ligeia Mare and Punga Mare basins (Fig. 16b). A Kraken-sized sea forms in that basin due to the evaporative scaling and the intermediate permeability aquifer surrounding the arid low latitudes regions of the basin, preventing the rapid removal of liquid in Kraken Mare to the subsurface. Nevertheless, there is a net loss of fluid from Kraken Mare due to subsurface flow throughout the Titan year. This is shown in the hydrograph for Kraken Mare (Fig. 16c), which predicts substantial surface runoff and precipitation from the high polar latitudes, and net removal of methane from evaporation and subsurface flow to the surrounding low latitude aquifer. This subsurface flow from Kraken Mare likely contributes to the hydrology of smaller surrounding lakes.

5. Discussion

5.1. Basin-scale models

For all permeability values, lakes at Titan's North Pole are predicted to remain stable over a Titan year. While lower permeability aquifers predict larger seasonal changes and the complete drying of some smaller lakes (< 100 km), large lakes are difficult to dry out as a result of both their large volume and their connection to the subsurface aquifers. The large sizes and lack of observed shoreline change at Titan's north polar region supports the interpretation that stable lakes are connected to a high or intermediate permeability aquifer. In contrast, the abundance of dry lakebed features (Hayes et al., 2008) supports the importance of long-term changes in the climate (Aharonson et al., 2009). The intermediate and high permeability aquifer models predict that subsurface flow into lakes comprises ~29–32% of the total fluid flux into the lakes, which is ~2 times that at lower permeability. For all permeabilities, the large contribution of direct precipitation to the lakes (~51% of the total influx) is a result of the arid climate and the assumed Budyko relationship that governs the amount of

Table 1

Summary of results and implications for the basin-scale and polar models.

Model results		Comparison with observations	Implications
Basin-scale models			
Low permeability (10^{-10} cm^2)	Large seasonal change in lake area and small scattered lakes perched at high elevations		
Intermediate permeability (10^{-8} cm^2)	Stable, large lakes filling topographic depressions due to the balance of evaporation and subsurface flow	Large north polar lakes and seas are observed to be stable with no discernable shoreline changes during the Cassini mission (Hayes et al., 2011)	Models favor subsurface flow in a high to intermediate permeability aquifer and show the importance of subsurface flow on Titan lakes and seas
High permeability (10^{-6} cm^2)			
Polar models			
High permeability	High rates of subsurface flow results in the rapid removal liquid from the system	Total lake area is significantly lower than the observed lake distribution without methane in the hydrological system and evaporation suppression over Kraken Mare	Needs unrealistically high aquifer recharge and runoff with evaporation suppression over Kraken Mare to form a Kraken Mare-sized sea
Intermediate permeability	Decreased subsurface flow results in a raised methane table and prevents removal of liquid from Kraken Mare	Fits the observed distribution but fails to form a Kraken Mare-sized lake without evaporation suppression	Intermediate permeability and a high permeability cap surrounded by an intermediate permeability models agrees with the observed lake distribution and form a Kraken Mare-sized sea when evaporation suppression is included
Polar cap	Diffused methane table at the high polar latitudes but flow to lower latitudes impeded by intermediate permeability aquifer surrounding the pole	Fits the observed distribution when a slight increase in runoff and recharge is included but fails to form a Kraken Mare-sized lake without evaporation suppression	
Low permeability		Models not run based on results from previous basin-scale model	

direct evaporation of the precipitation that falls on the land surface. While low permeability models predict lake areas $< 10^3 \text{ km}^2$, high and intermediate permeability models predict a large sea intermediate in size between Jingpo Lacus ($1.7 \times 10^4 \text{ km}^2$) and Punga Mare ($4.0 \times 10^4 \text{ km}^2$) but fail to produce a Ligeia Mare-sized sea. The better agreement between the size and stability of lakes predicted by the high and intermediate permeability models and the observed lakes suggests that a significant component of subsurface flow contributes to the hydrology on Titan. The extreme limit of zero permeability would be equivalent to the case in which there is no subsurface component to Titan's hydrological cycle and the formation and stability of lakes is driven exclusively by runoff, direct precipitation, and evaporation at the lake surface. Thus, the fact that the low permeability models do not match the observed sizes and stability of lakes effectively rules out the scenario in which there is no subsurface component to Titan's hydrological cycle.

5.2. Polar models

Polar models at both high and intermediate permeability require a dramatically decreased evaporation potential (~1% of the rate predicted by the GCM) over Kraken Mare in order to form a sufficiently large sea. This is easily understood as a consequence of the dramatic increase in evaporation rates below 75°N in the southernmost reaches of the basin, which exceeds the input to the basin from subsurface flow, runoff, and direct precipitation from the higher latitudes. The decreased evaporation over Kraken Mare can be brought about by the combination of an increase in the concentration of ethane or organic solutes within Kraken Mare (Tokano, 2009; Lorenz, 2014), and a lake effect on the climate over a large sea resulting in the suppression of evaporation by evaporative cooling (Tokano, 2009). These effects are important to the stability of Kraken Mare at lower latitudes. While models with an increased aquifer recharge and runoff and smaller evaporation suppression can result in a Kraken-sized sea, these models fail to fit the observed lake distribution outside of Kraken Mare.

Furthermore, models with a high permeability aquifer at the north polar region result in the rapid removal of liquid from the high polar latitudes to the dry lower polar latitudes resulting in a lower total lake area at the north polar region even when evaporative suppression is accounted for over Kraken Mare. While basin-scale models necessitate a high to intermediate permeability in order to stabilize large lakes, at long distance scales, higher permeability values can, impede lake formation at the high polar latitudes and within Kraken Mare. Models with an intermediate permeability aquifer or a high permeability aquifer surrounded by an intermediate permeability aquifer with evaporation suppression over Kraken Mare provide general agreement with the observed lake distribution at the north polar region. This suggests that while the higher polar latitudes may be characterized by dissolution in the subsurface leading to enhanced subsurface flow, similar processes may not be at work at the lower polar latitudes where an intermediate to low permeability aquifer is required to stabilize Kraken Mare and the large seas in the arctic lake district. More importantly, we have shown that by comparing hydrological models to the observed distribution of lakes, we can shed light on the nature of the full hydrological cycle, from the subsurface to the atmosphere (Table 1).

6. Summary and conclusions

Titan is the only body, besides the Earth, with an active hydrological cycle. Cassini observations reveal an abundance of hydrocarbon lakes and seas in the north polar region (Stofan et al., 2007) resulting from the more temperate polar climate in comparison to the hyper-arid lower latitudes. By analogy with Earth and Mars, it appears likely that subsurface flow may feature prominently in the hydrology of Titan. Although we have very few constraints on the properties of Titan's surface and subsurface that govern the transport of methane across and beneath the surface, the distribution of lakes provides an important observational constraint for comparison to models, which in turn can provide insight into the unseen details of Titan's subsurface hydrology.

Basin-scale models show that high latitude Titan lakes connected to an unconfined aquifer with high ($\sim 10^{-6}$ cm 2) to intermediate ($\sim 10^{-8}$ cm 2) permeability are predicted to remain stable on the surface over a Titan year in a semi-arid climate similar to polar regions of Titan, and show little to no seasonal shoreline change, consistent with observations. Lakes of a range of sizes up to and exceeding 10 4 km 2 form for these permeabilities, in agreement with the observed sizes of lakes. In contrast, lower permeability values ($\sim 10^{-10}$ cm 2) predict substantial seasonal changes in lake area and an abundance of smaller perched lakes rather than a mix of small lakes and large seas, in conflict with the observations. Thus, these basin-scale models support the importance of subsurface flow through intermediate to high permeability aquifers in Titan's hydrological cycle.

Large-scale polar models with latitudinally varying climates and topography with imposed basins allow for a more direct comparison of the model results with observations for the distribution of lakes with latitude and the formation of the large seas. Intermediate permeability models predict abundant lakes at high polar latitudes, but a deficit of lakes at lower polar latitudes. High permeability models predict a deficit of high latitude lakes, but do allow a few lakes to form at lower polar latitudes due to subsurface flow from temperate high polar latitudes to hyper-arid low latitude topographic depressions. Increased recharge and runoff result in an increase in the total lake area and partially fill the larger basins in the high polar latitudes. However, all of these models both fail to produce a Kraken-sized sea and disagree with the observed latitudinal lake distribution.

Observational evidence indicates high latitudes are characterized by material of a different composition at the surface, as well as putative karstic features that are likely associated with increased permeability. Inclusion of a higher permeability polar cap surrounded by an intermediate permeability aquifer at lower polar latitudes raises the methane table and allows subsurface flow at the higher polar latitudes while preventing appreciable loss of methane to the low latitudes as well as the aquifer surrounding Kraken Mare. In this model, the combination of a somewhat increased recharge and runoff fraction and a permeability drop at lower polar latitudes results in a good agreement between the predicted and observed lake area distribution. This model provides a slightly better fit to the distribution of small lower latitude lakes than the uniform intermediate permeability model with enhanced runoff and recharge and evaporation suppression over Kraken Mare.

These model results indicate that subsurface flow is an essential component to the hydrological cycle on Titan. Subsurface flow directly accounts for approximately 1/3 of the influx into typical Titan lakes in our models. Moreover, subsurface flow plays a critical role in redistributing fluid across the surface over a range of spatial scales. Over short to intermediate length scales, subsurface flow acts as both a source and sink of fluid in order to produce the observed distribution of lakes. Infiltration and subsurface transport are necessary to prevent the formation and stability of a myriad of small lake perched at high elevation in every closed topographic depression. At the same time, subsurface flow provides a critical source of fluid to lakes, helping to stabilize them during periods of high evaporation so as to reduce the magnitude of seasonal changes. However, over long distances, the effect of subsurface flow is contrary to observations – long distance subsurface flow from temperate high latitudes to arid mid-latitudes impedes lake formation in the arctic lake district. To balance these competing effects, either a uniform aquifer of intermediate permeability or a high permeability aquifer at the pole surrounded by an intermediate permeability aquifer is required to reproduce the sizes and latitudinal distribution of Titan's lakes.

The models that best match the observed distribution invoke either a similar scaling law to partition precipitation between direct evaporation and recharge/runoff as that typically applied on Earth (uniform intermediate permeability model) or scale the recharge and runoff fraction by a factor of 3 (high permeability cap model). This suggests that the net effect of microscale processes in the soil layer on the fate of precipitation falling on the surface on Titan are of the same order of magnitude as on Earth. This inference is surprising given the important role of biologically-derived organic material in Earth's soils, and may suggest that atmospherically derived organics play a similar role in Titan's soils.

Our work also reveals the critical role that some form of evaporation suppression over Kraken Mare plays in the stabilization of that sea, despite its spanning latitudinal climate zones ranging from temperate to hyper-arid. The necessity of a decreased evaporation potential over Kraken Mare in order to create a Kraken-sized sea suggests that Kraken Mare may be influenced by the effects of both ethane and/or dissolved organic solutes as suggested by previous studies (Tokano, 2009; Lorenz, 2014; Tan et al., 2015) and an evaporative cooling effect not accounted for at the dry, lower polar latitudes in the GCM, preventing appreciable evaporation over Kraken Mare. This problem is exacerbated by subsurface flow, which acts as a net sink of fluids flowing from Kraken to the surroundings in the lower latitude reaches of the sea.

Although this work has made significant advances in representing the full hydrological cycle of Titan, it nevertheless relies on a number of assumptions and simplifications. The true topography of Titan is not likely to be purely fractal in character. Erosion, deposition, and dissolution appear to have modified the landscape in a manner that would affect both the scale of overland flow and the relief surrounding lakes and seas. However, the approximate agreement between lengths of drainage basins in the model and on Titan and the immature fluvial state of much of the Titan landscape suggests that the fractal terrain is a reasonable simplification. Although preliminary models using diffused landscapes found similar results to those presented in this work, future work should include the effects of landscape evolution on Titan. Dissolution also appears to play a role in the formation of steep-sided lakes and may influence the distribution of small lakes. Given that the basin-scale models focused on the hydrology of the large seas, these small steep-sided depressions will have little influence on the model results for the basin-scale models. The metric that the polar models were compared against (the latitudinal distribution of lakes) is dependent on the balance of fluxes into and out of the model, which will be controlled by the assumed recharge and runoff, and evaporation suppression. Thus, a lack of explicit steep-sided depressions in the polar models will only have a slight influence on the latitudinal distribution of lakes. Future work will investigate the influence of dissolution and deviations from Darcy flow in the subsurface. The GCM included a sophisticated treatment of the methane cycle, but did not include the effects of large seas on the climate. Future work should include known lakes and seas in the GCM, as well as the effects of the surface topography. Our models also assumed the liquid to be pure methane. Although the effect of solutes on the viscosity is minor in comparison to the uncertainty in the permeability, solutes can play an important role in the suppression of evaporation. Nevertheless, our simplified treatment of evaporation suppression over Kraken Mare enabled us to quantify the magnitude of the combined effects of the concentration of solutes in the sea and the impact of the sea on the local climate. The conclusion that decreased evaporation over Kraken Mare remains robust even with our simplified treatment of evaporation suppression.

In summary, while there is clear evidence for the surface and atmospheric components of Titan's hydrological cycle, there are no direct observations of the subsurface component. By using

models that integrate the atmospheric, surface, and subsurface components of Titan's hydrological cycle, and comparing the results to the observed sizes and spatial distribution of lakes, we have made inferences regarding the nature of Titan's subsurface and surface hydrology. Subsurface flow plays a critical role in governing the sizes, distribution, and stability of lakes and seas on Titan.

Acknowledgments

This work was supported by NASA Outer Planets Research Program grant NNX10AQ06G to JCAH. We are grateful to Reed Maxwell and Dave Benson for discussions that contributed to this work, and to Devon Burr and Alex Hayes for their thorough and thoughtful reviews of this manuscript. Some of this research was carried out at the California Institute of Technology Jet Propulsion Laboratory under a contract from NASA.

References

- Aharonson, O., Hayes, A.G., Lunine, J.I., et al., 2009. An asymmetric distribution of lakes on Titan as a possible consequence of orbital forcing. *Nat. Geosci.* 2, 851–854. doi:[10.1038/ngeo698](https://doi.org/10.1038/ngeo698).
- Black, B.A., Perron, J.T., Burr, D.M., et al., 2012. Estimating erosional exhumation on Titan from drainage network morphology. *J. Geophys. Res.* 117, E08006. doi:[10.1029/2012JE004085](https://doi.org/10.1029/2012JE004085).
- Brown, R.H., Soderblom, L.A., Soderblom, J.M., et al., 2008. The identification of liquid ethane in Titan's Ontario Lacus. *Nature* 454, 607–610. doi:[10.1038/nature07100](https://doi.org/10.1038/nature07100).
- Budyko, M., 1974. *Climate and Life*. Academic Press ISBN:9780080954530.
- Burr, D.M., Emery, J.P., Lorenz, R.D., et al., 2006. Sediment transport by liquid surficial flow: application to Titan. *Icarus* 181, 235–242. doi:[10.1016/j.icarus.2005.11.012](https://doi.org/10.1016/j.icarus.2005.11.012).
- Burr, D.M., Jacobsen, R.E., Roth, D.L., et al., 2009. Fluvial network analysis on Titan: evidence for subsurface structures and west-to-east wind flow, southwestern Xanadu. *Geophys. Res. Lett.* 36, L22203. doi:[10.1029/2009GL040909](https://doi.org/10.1029/2009GL040909).
- Burr, D.M., Perron, T.J., Lamb, M.P., et al., 2013. Fluvial features on Titan: insights from morphology and modeling. *Geol. Soc. Am. Bull.* 125, 299–321. doi:[10.1130/B30612.1](https://doi.org/10.1130/B30612.1).
- Campbell, B.A., 2002. *Radar Remote Sensing of Planetary Surfaces*, first ed. Cambridge University Press. ISBN:9780521189651.
- Cartwright, R., Clayton, J.A., Kirk, R.L., 2011. Channel morphometry, sediment transport, and implications for tectonic activity and surficial ages of Titan basins. *Icarus* 214, 561–570. doi:[10.1016/j.icarus.2011.03.011](https://doi.org/10.1016/j.icarus.2011.03.011).
- Cornet, T., Bourgeois, O., Le Mouelic, S., et al., 2012. Edge detection applied to Cassini images reveals no measurable displacement of Ontario Lacus' margin between 2005 and 2010. *J. Geophys. Res.* 117, E07005. doi:[10.1029/2012JE004073](https://doi.org/10.1029/2012JE004073).
- Cornet, T., Cordier, D., Bahers, T.L., et al., 2015. Dissolution on Titan and on Earth: Toward the age of Titan's karstic landscapes. *J. Geophys. Res. Planets* 120, 1044–1074. doi:[10.1002/2014JE004738](https://doi.org/10.1002/2014JE004738).
- Cunge, J.A., 1969. On the subject of the flood propagation computation method. *J. Hydraul. Res.* 7, 205–230.
- Dooce, J.C.I., 1973. *Linear Theory of Hydrologic Systems*. Agri. Res. Serv. Tech. Bull. 1468, 1–327.
- Elachi, C., Wall, S., Allison, M., et al., 2005. Cassini Radar views the surface of Titan. *Science* 308, 970–974. doi:[10.1126/science.1109919](https://doi.org/10.1126/science.1109919).
- Fan, Y., Miguez-Macho, G., Weaver, C.P., et al., 2007. Incorporating water table dynamics in climate modeling: 1. Water table observations and equilibrium water table simulations. *J. Geophys. Res.* 112, D10125. doi:[10.1029/2006JD008111](https://doi.org/10.1029/2006JD008111).
- Fournier, A., Fussell, A.D., Carpenter, L., 1982. Computer rendering of stochastic models. *Commun. ACM* 25, 371–384.
- Freeze, R.A., Witherspoon, P.A., 1967. Theoretical analysis of regional groundwater flow: 2. Effect of water-table configuration and subsurface permeability variation. *Water Resour. Res.* 3, 623–634.
- Freeze, R.A., Cherry, J.A., 1979. *Groundwater*. Prentice Hall ISBN:9780133653120.
- Gammon, P.H., Kieft, H., Clouter, M.J., et al., 1983. Elastic constants of artificial and natural ice samples by Brillouin spectroscopy. *J. Glaciol.* 29, 433–460.
- Hanna, J.C., Phillips, R., 2005. Hydrological modeling of the Martian crust with application to the pressurization of aquifers. *J. Geophys. Res.* 110, E01004. doi:[10.1029/2004JE002330](https://doi.org/10.1029/2004JE002330).
- Harbaugh, A.W., 2005. *MODFLOW-2005, The U.S. geological survey modular ground-water model—the ground-water flow process*. U.S. Geological Survey Techniques and Methods 6-A16. U.S. Geological Survey, Reston, Virginia.
- Hayes, A., Aharonson, O., Callahan, P., et al., 2008. Hydrocarbon lakes on Titan: Distribution and interaction with a porous regolith. *Geophys. Res. Lett.* 35, L09204. doi:[10.1029/2008GL033409](https://doi.org/10.1029/2008GL033409).
- Hayes, A.G., Aharonson, O., Lunine, J.I., et al., 2011. Transient surface liquid in Titan's polar regions from Cassini. *Icarus* 211, 655–671. doi:[10.1016/j.icarus.2010.08.017](https://doi.org/10.1016/j.icarus.2010.08.017).
- Hayes, A.G., Lorenz, R.D., Donelan, M.A., et al., 2013. Wind driven capillary-gravity waves on Titan's lakes: Hard to detect or non-existent? *Icarus* 225, 403–412. doi:[10.1016/j.icarus.2013.04.004](https://doi.org/10.1016/j.icarus.2013.04.004).
- Heath, R.C., 1983. Basic ground-water hydrology. U. S. Geological Survey Water-Supply Paper 2220, 86 p. ISBN:0607689730.
- Hofgartner, J.D., Hayes, A.G., Lunine, J.I., et al., 2014. Transient features in Titan sea. *Nat. Geosci.* 7, 493–496. doi:[10.1038/ngeo2190](https://doi.org/10.1038/ngeo2190).
- Jaumann, R., Brown, R.H., Stephan, K., et al., 2008. Fluvial erosion and post-erosional processes on Titan. *Icarus* 197, 526–538. doi:[10.1016/j.icarus.2008.06.002](https://doi.org/10.1016/j.icarus.2008.06.002).
- Kirk, R.L., Howington-Kraus, E., Redding, B., et al., 2013. Topographic mapping of Titan: Completion of a global radargrammetric control network opens the floodgates for stereo DTM production. In: *Proceedings of Lunar and Planetary Science Conference*, 44, p. 2898.
- Krasnopolsky, V.A., 2009. A photochemical model of Titan's atmosphere and ionosphere. *Icarus* 201, 226–256. doi:[10.1016/j.icarus.2008.12.038](https://doi.org/10.1016/j.icarus.2008.12.038).
- Langhans, M.H., Jaumann, R., Stephan, K., et al., 2012. Titan's fluvial valleys: Morphology, distribution, and spectral properties. *Planet. Space Sci.* 60, 34–51. doi:[10.1016/j.pss.2011.01.020](https://doi.org/10.1016/j.pss.2011.01.020).
- Lavvas, P.P., Coustenis, A., Vardavas, I.M., 2008. Coupling photochemistry with haze formation in Titan's atmosphere, Part II: Results and validation with Cassini/Huygens data. *Planet. Space Sci.* 56, 67–99. doi:[10.1016/j.pss.2007.05.027](https://doi.org/10.1016/j.pss.2007.05.027).
- Le Gall, A., Janssen, M.A., Paillou, P., et al., 2010. Radar-bright channels on Titan. *Icarus* 207, 948–958. doi:[10.1016/j.icarus.2009.12.027](https://doi.org/10.1016/j.icarus.2009.12.027).
- Lopes, R.M.C., Mitchell, K.L., Stofan, E.R., et al., 2007. Cryovolcanic features on Titan's surface as revealed by the Cassini Titan radar mapper. *Icarus* 186, 395–412. doi:[10.1016/j.icarus.2006.09.006](https://doi.org/10.1016/j.icarus.2006.09.006).
- Lopes, R.M.C., Kirk, R.L., Mitchell, K.L., et al., 2013. Cryovolcanism on Titan: New results from Cassini radar and VIMS. *J. Geophys. Res.* 118, 416–435. doi:[10.1002/jgre.20062](https://doi.org/10.1002/jgre.20062).
- Lora, J.M., Lunine, J.I., Russell, J.L., et al., 2014. Simulations of Titan's paleoclimate. *Icarus* 243, 264–273. doi:[10.1016/j.icarus.2014.08.042](https://doi.org/10.1016/j.icarus.2014.08.042).
- Lorenz, R.D., Lemmon, M.T., Smith, P.H., 1999. Seasonal change on Titan observed with the Hubble space telescope. *Icarus* 142, 391–401.
- Lorenz, R.D., Kraal, E., Asphaug, E., et al., 2003. The Seas of Titan. *Eos* 84, 131–132.
- Lorenz, R.D., Lopes, R.M., Paganelli, F., et al. the Cassini radar team, 2008. Fluvial channels on Titan: Initial Cassini radar observations. *Planet. Space Sci.* 56, 1132–1144. doi:[10.1016/j.pss.2008.02.009](https://doi.org/10.1016/j.pss.2008.02.009).
- Lorenz, R.D., Mitchell, K.L., Kirk, R.L., et al., 2008. Titan's inventory of organic surface materials. *Geophys. Res. Lett.* 35, L02206. doi:[10.1029/2007GL032118](https://doi.org/10.1029/2007GL032118).
- Lorenz, R.D., Newman, C., Lunine, J.I., 2010. Threshold of wave generation on Titan's lakes and seas: Effect of viscosity and implications for Cassini observations. *Icarus* 207, 932–937. doi:[10.1016/j.icarus.2009.12.004](https://doi.org/10.1016/j.icarus.2009.12.004).
- Lorenz, R.D., 2014. The flushing of Ligeia: Composition variations across Titan's seas in a simple hydrological model. *Geophys. Res. Lett.* 41, doi:[10.1002/2014GL061133](https://doi.org/10.1002/2014GL061133).
- Lucas, A., Aharonson, O., Deledalle, C., et al., 2014. Insights into Titan's geology and hydrology based on enhanced image processing of Cassini radar data. *J. Geophys. Res. Planets* 119, 2149–2166. doi:[10.1002/2013JE004584](https://doi.org/10.1002/2013JE004584).
- Lunine, J.I., Stevenson, D.J., Yung, Y.L., 1983. Ethane ocean on Titan. *Science* 222, 1229–1230. doi:[10.1126/science.222.4629.1229](https://doi.org/10.1126/science.222.4629.1229).
- Malaska, M.J., Hodys, R., 2014. Dissolution of benzene, naphthalene, and biphenyl in a simulated Titan lake. *Icarus* 242, 74–81. doi:[10.1016/j.icarus.2014.07.022](https://doi.org/10.1016/j.icarus.2014.07.022).
- Mandelbrot, B., 1982. *The Fractal Geometry of Nature*, first ed. W. H. Freeman and Company, ISBN:9780716711865.
- Manning, C.E., Ingebritsen, S.E., 1999. Permeability of the continental crust: Implications of geothermal data and metamorphic systems. *Rev. Geophys.* 37, 127–150. doi:[10.1029/1998RG900002](https://doi.org/10.1029/1998RG900002).
- Mastrogiosse, M., Poggiali, V., Hayes, A., et al., 2014. The bathymetry of a Titan sea. *Geophys. Res. Lett.* 41, 1432–1437. doi:[10.1002/2013GL058618](https://doi.org/10.1002/2013GL058618).
- Maxwell, R.M., Miller, N.L., 2005. Development of a coupled land surface and groundwater model. *J. Hydrometeorol.* 6, 233–247.
- McMahon, T.A., Peel, M.C., Pegram, G.G.S., et al., 2011. A simple methodology for estimating mean and variability of annual runoff and reservoir yield under present and future climates. *J. Hydrometeorol.* 12, 135–146. doi:[10.1175/2010JHM1288.1](https://doi.org/10.1175/2010JHM1288.1).
- Mitchell, J.L., Pierrehumbert, R.T., Frierson, M.W., et al., 2006. The dynamics behind Titan's methane clouds. *Proc. Natl. Acad. Sci.* 103, 18421–18426. doi:[10.1073/pnas.0605074103](https://doi.org/10.1073/pnas.0605074103).
- Mitchell, K.L., Lopes, R.M.C., Radebaugh, J., et al., 2008. The formation of high latitude karst Lakes on Titan and implications for the existence of polar caps. In: *Proceedings of Lunar and Planetary Science Conference*, 39, p. 2170.
- Mitchell, K.L., Barmatz, M.B., Jamieson, C.S., et al., 2015. Laboratory measurements of cryogenic liquid alkane microwave absorptivity and implications for the composition of Ligeia Mare, Titan. *Geophys. Res. Lett.* 42, doi:[10.1002/2014GL059475](https://doi.org/10.1002/2014GL059475).
- Mitri, G., Showman, A.P., Lunine, J.I., et al., 2007. Hydrocarbon lakes on Titan. *Icarus* 186, 385–394. doi:[10.1016/j.icarus.2006.09.004](https://doi.org/10.1016/j.icarus.2006.09.004).
- Newman, C.E., Lee, C., Lian, Y., et al., 2011. Stratospheric superrotation in the Titan-WRF model. *Icarus* 213, 636–654. doi:[10.1016/j.icarus.2011.03.025](https://doi.org/10.1016/j.icarus.2011.03.025).
- Newman, C.E., 2015. Planetary science: Stormy origins of Titan's dunes. *Nat. Geosci.* 8, 334–335. doi:[10.1038/ngeo2423](https://doi.org/10.1038/ngeo2423).
- Niemann, H.B., Atreya, S.K., Bauer, S.J., et al., 2005. The abundances of constituents of Titan's atmosphere from the GCMS instrument on the Huygens probe. *Nature* 438, 779–784. doi:[10.1038/nature04122](https://doi.org/10.1038/nature04122).
- Overton, D.E., 1970. Route or convolute? *Water Resour. Res.* 6, 43–52.
- Perron, T.J., Lamb, M.P., Koven, C.D., et al., 2006. Valley formation and methane precipitation rates on Titan. *J. Geophys. Res.* 111, E11001. doi:[10.1029/2005JE002602](https://doi.org/10.1029/2005JE002602).
- Porco, C.C., Baker, E., Barbara, J., et al., 2005. Imaging of Titan from the Cassini spacecraft. *Nature* 434, 159–168. doi:[10.1038/nature03436](https://doi.org/10.1038/nature03436).

- Renard, F., Gratier, J., Jamtveit, B., 2000. Kinetics of crack-sealing, intergranular pressure solution, and compaction around active faults. *J. Struct. Geol.* 22, 1395–1407. doi:[10.1016/S0191-8141\(00\)00064-X](https://doi.org/10.1016/S0191-8141(00)00064-X).
- Richardson, M.I., Toigo, A.D., Newman, C.E., 2007. PlanetWRF: A general purpose, local to global numerical model for planetary atmospheric and climate dynamics. *J. Geophys. Res.* 112, E09001. doi:[10.1029/2006JE002825](https://doi.org/10.1029/2006JE002825).
- Schaller, E., Brown, M., Roe, H., et al., 2006. Dissipation of Titan's south polar clouds. *Icarus* 184, 517–523. doi:[10.1016/j.icarus.2006.05.025](https://doi.org/10.1016/j.icarus.2006.05.025).
- Schneider, T., Graves, S.D.B., Schaller, E.L., et al., 2012. Polar methane accumulation and rainstorms on Titan from simulations of the methane cycle. *Nature* 481, 58–61. doi:[10.1038/nature10666](https://doi.org/10.1038/nature10666).
- Sharma, P., Byrne, S., 2010. Constraints on Titan's topography through fractal analysis of shorelines. *Icarus* 209, 723–737. doi:[10.1016/j.icarus.2010.04.023](https://doi.org/10.1016/j.icarus.2010.04.023).
- Snow, D.T., 1970. The frequency and apertures of fractures in rock. *Int. J. Rock Mech. Min. Sci.* 7, 23–40.
- Sotin, C., Mielke, R., Choukroun, M., et al., 2009. Ice-hydrocarbon interaction under Titan-like conditions: Implications for the carbon cycle on Titan. In: Proceedings of Lunar and Planetary Science Conference, 40, p. 2088.
- Stiles, B.W., Hensley, S., Gim, Y., et al. the Cassini radar team, 2009. Determining Titan surface topography from Cassini SAR data. *Icarus* 202, 584–598. doi:[10.1016/j.icarus.2009.03.032](https://doi.org/10.1016/j.icarus.2009.03.032).
- Stofan, E.R., Elachi, C., Lunine, J.I., et al., 2007. The lakes of Titan. *Nature* 445, 61–64. doi:[10.1038/nature05438](https://doi.org/10.1038/nature05438).
- Tan, S.P., Kargel, J.S., Marion, G.M., 2013. Titan's atmosphere and surface liquid: New calculation using statistical fluid theory. *Icarus* 222, 53–72. doi:[10.1016/j.icarus.2012.10.032](https://doi.org/10.1016/j.icarus.2012.10.032).
- Tan, S.P., Kargel, J.S., Jennings, D.E., et al., 2015. Titan's liquids: Exotic behavior and its implications on global fluid circulation. *Icarus* 250, 64–75. doi:[10.1016/j.icarus.2014.11.029](https://doi.org/10.1016/j.icarus.2014.11.029).
- Tokano, T., Neubauer, F.M., Laube, M., 2001. Three-dimensional modeling of the tropospheric methane cycle on Titan. *Icarus* 153, 130–147. doi:[10.1006/icar.2001.6659](https://doi.org/10.1006/icar.2001.6659).
- Tokano, T., 2009. Impact of seas/lakes on polar meteorology on Titan: Simulations by a coupled GCM-Sea model. *Icarus* 204, 619–636. doi:[10.1016/j.icarus.2009.07.032](https://doi.org/10.1016/j.icarus.2009.07.032).
- Turtle, E.P., Perry, J.E., McEwen, A.S., et al., 2009. Cassini imaging of Titan's high-latitude lakes, clouds, and south-polar surface changes. *Geophys. Res. Lett.* 36, L02204. doi:[10.1029/2008GL036186](https://doi.org/10.1029/2008GL036186).
- Turtle, E.P., Perry, J.E., Hayes, A.G., et al., 2011. Shoreline retreat at Titan's Ontario Lacus and Arrakis Planitia from Cassini imaging science subsystem observations. *Icarus* 212, 957–959. doi:[10.1016/j.icarus.2011.02.005](https://doi.org/10.1016/j.icarus.2011.02.005).
- Turtle, E.P., Perry, J.E., McEwen, A.S., et al., 2013. ISS observations of Titan's northern lakes and evidence for a north-polar surface unit. In: Proceedings of AGU Fall Meeting, p. D1897.
- Wang, M., Hjelmfelt, A.T., 1998. DEM based overland flow routing model. *J. Hydrol. Eng.* 3, 1–8.
- Watt, E.W., Chow, A.K.C., 1985. A general expression for basin lag time. *Can. J. Civil Eng.* 12, 294–300.
- Webb, J.A., James, J.M., 2006. Karst evolution of the Nullarbor Plain, Australia. *Geol. Soc. Am. Spec. Pap.* 404, 65–78. doi:[10.1130/2006.2404\(07\)](https://doi.org/10.1130/2006.2404(07)).
- Zarnecki, J.C., Leese, M.R., Hathi, B., et al., 2005. A soft solid surface on Titan as revealed by the Huygens surface science package. *Nature* 438, 792–795. doi:[10.1038/nature04211](https://doi.org/10.1038/nature04211).